Cardiac myofibroblast engulfment of dead cells facilitates recovery after myocardial infarction

Michio Nakaya,[1] Kenji Watari,[1] Mitsuru Tajima,[1] Takeo Nakaya,[2,3] Shoichi Matsuda,[1] Hiroki Ohara,[1] Hiroaki Nishihara,[1] Hiroshi Yamaguchi,[4,5] Akiko Hashimoto,[1] Mitsuho Nishida,[1] Akiomi Nagasaka,[1] Yuma Horii,[1] Hiroki Ono,[1] Gentaro Iribe,[6] Ryuji Inoue,[7] Makoto Tsuda,[8] Kazuhide Inoue,[8] Akira Tanaka,[2] Masahiko Kuroda,[3] Shigekazu Nagata,[4,5] and Hitoshi Kurose[1]

[1]Department of Pharmacology and Toxicology, Graduate School of Pharmaceutical Sciences, Kyushu University, Fukuoka, Japan. [2]Department of Pathology, Jichi Medical University, Tochigi, Japan. [3]Department of Molecular Pathology, Tokyo Medical University, Tokyo, Japan. [4]Department of Medical Chemistry, Graduate School of Medicine, Kyoto University, Kyoto, Japan. [5]Core Research for Evolutional Science and Technology, Japan Science and Technology Agency, Tokyo, Japan. [6]Department of Cardiovascular Physiology, Okayama University Graduate School of Medicine, Dentistry and Pharmaceutical Sciences, Okayama, Japan. [7]Department of Physiology, School of Medicine, Fukuoka University, Fukuoka, Japan. [8]Molecular and System Pharmacology, Graduate School of Pharmaceutical Sciences, Kyushu University, Fukuoka, Japan.

Myocardial infarction (MI) results in the generation of dead cells in the infarcted area. These cells are swiftly removed by phagocytes to minimize inflammation and limit expansion of the damaged area. However, the types of cells and molecules responsible for the engulfment of dead cells in the infarcted area remain largely unknown. In this study, we demonstrated that cardiac myofibroblasts, which execute tissue fibrosis by producing extracellular matrix proteins, efficiently engulf dead cells. Furthermore, we identified a population of cardiac myofibroblasts that appears in the heart after MI in humans and mice. We found that these cardiac myofibroblasts secrete milk fat globule-epidermal growth factor 8 (MFG-E8), which promotes apoptotic engulfment, and determined that serum response factor is important for MFG-E8 production in myofibroblasts. Following MFG-E8–mediated engulfment of apoptotic cells, myofibroblasts acquired antiinflammatory properties. MFG-E8 deficiency in mice led to the accumulation of unengulfed dead cells after MI, resulting in exacerbated inflammatory responses and a substantial decrease in survival. Moreover, MFG-E8 administration into infarcted hearts restored cardiac function and morphology. MFG-E8–producing myofibroblasts mainly originated from resident cardiac fibroblasts and cells that underwent endothelial-mesenchymal transition in the heart. Together, our results reveal previously unrecognized roles of myofibroblasts in regulating apoptotic engulfment and a fundamental importance of these cells in recovery from MI.

Introduction

Myocardial infarction (MI) is a major disease worldwide (1, 2). Following MI, cardiomyocytes receiving blood supply from occluded blood vessels die rapidly due to the shortage of oxygen and nutrients (3, 4). These dead cells release noxious intracellular contents that induce secondary cell death and inflammatory responses (5–7). Therefore, dead cells generated following MI are swiftly engulfed to prevent the expansion of the damaged area. Leakage of cellular contents from dead cells triggers the recruitment of inflammatory cells to the infarcted area (5). These inflammatory cells, such as macrophages and dendritic cells, have long been considered responsible for engulfment (5, 8). However, the cell types that mediate the engulfment of dead cardiomyocytes generated following MI and the molecular mechanisms underlying engulfment remain unknown.

Reparative responses also occur at the infarcted area (9). To prevent cardiac rupture caused by the loss of cardiomyocytes, the area occupied by dead cardiomyocytes is rapidly filled with collagen and extracellular matrix proteins produced by myofibroblasts. Myofibroblasts have been reported to initiate protein secretion only when they receive signals from activated inflammatory cells (10). In addition, myofibroblasts are not normally present, but rather appear in damaged tissues following differentiation from several cell types in response to inflammation (11–13). In failed hearts, cardiac myofibroblasts differentiate from 5 reported cell types: bone marrow–derived cells, pericytes, cells that have undergone epithelial-mesenchymal transition (EMT), those that have undergone endothelial-mesenchymal transition (EndMT), and resident fibroblasts (12, 14). However, the functional differences between myofibroblasts with different origins remain to be clarified (12–14).

We report that cardiac myofibroblasts execute the engulfment of dead cells generated following MI, a task previously believed to be performed only by infiltrating inflammatory cells. Engulfment by myofibroblasts was mediated by milk fat globule-epidermal growth factor 8 (MFG-E8), a protein known to promote apoptotic engulfment. MFG-E8 binds to both phosphatidylserine on dead cells and the integrin receptor $\alpha_v\beta_5$ on phagocytes, acting as a bridging molecule (15, 16). MFG-E8 was produced by myofibroblasts, and MFG-E8 production in these cells involved the TGF-β/serum response factor (SRF) pathway. MFG-E8–positive myofibroblasts were also found in infarcted areas of patients with MI. MFG-E8–deficient mice displayed an exacerbated inflammatory response and reduced survival after MI due to the accumulation of dead cells. Importantly, MFG-E8

Conflict of interest: The authors have declared that no conflict of interest exists.
Submitted: July 17, 2015; **Accepted:** October 20, 2016.
Reference information: *J Clin Invest*. 2017;127(1):383–401. doi:10.1172/JCI83822.

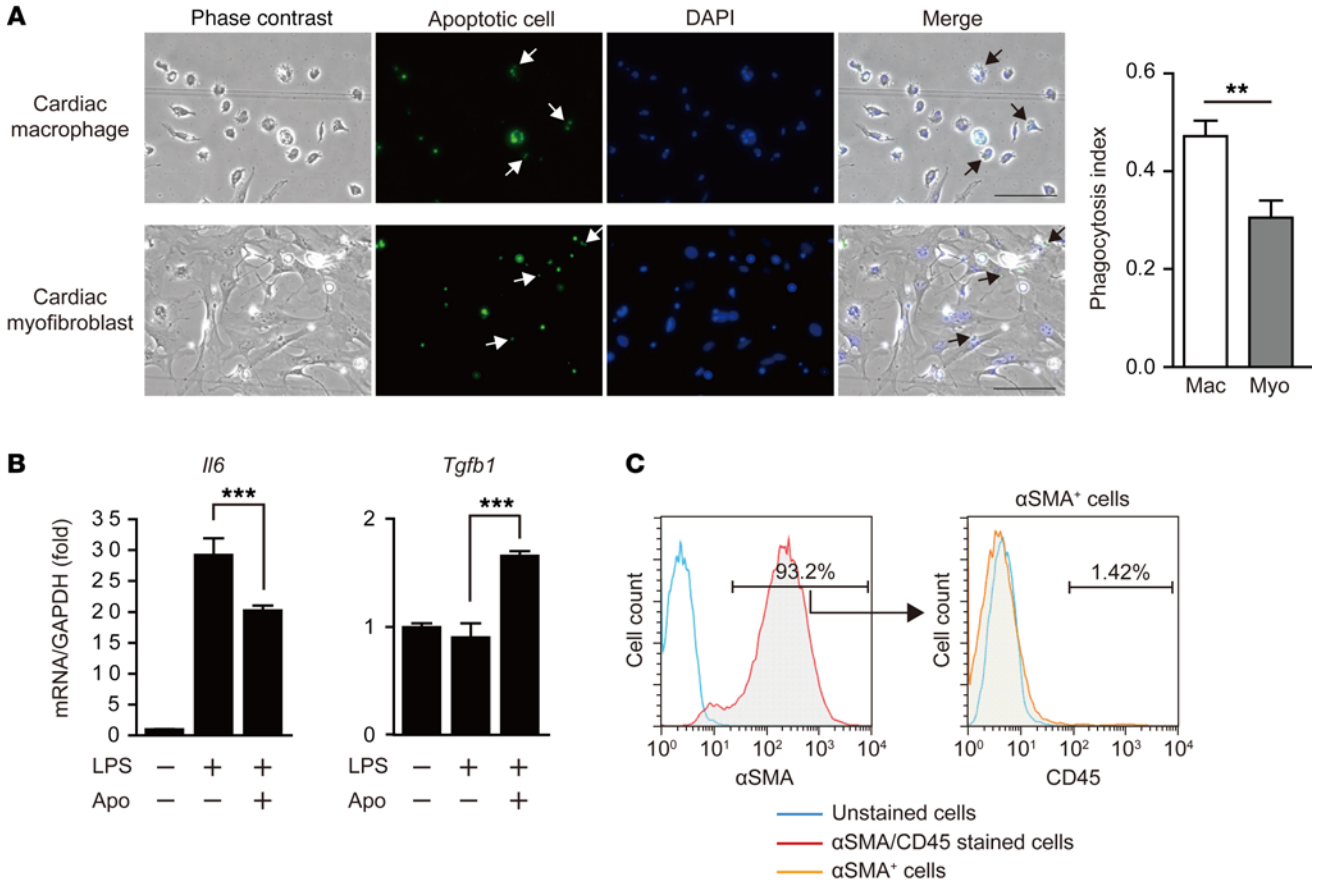

Figure 1. Cardiac myofibroblasts engulf dead cells ex vivo. (**A**) Ex vivo phagocytosis assay of apoptotic cells. Cardiac macrophages and myofibroblasts isolated from WT mice that underwent MI were exposed to apoptotic cells (green) (n = 3). The numbers of engulfed apoptotic cells per cardiac macrophage (Mac) and myofibroblast (Myo) are shown. Images were taken at 12–15 randomly selected fields. Arrows indicate engulfed apoptotic cells. Scale bar: 100 μm. Original magnification, ×40. (**B**) mRNA expression levels of *Il6* or *Tgfb1* in myofibroblasts treated with LPS after apoptotic engulfment. Cardiac myofibroblasts cocultured with (+) or without (–) apoptotic thymocytes (Apo) for 2 hours were treated with (+) or without (–) LPS at 1 μg/ml for 24 hours (n = 4). (**C**) αSMA-positive myofibroblasts did not express CD45. The cells collected from infarcted mouse hearts as myofibroblasts were harvested by treatment with accutase and immediately stained with antibodies for αSMA and CD45. Error bars represent the mean ± SEM. (**A**) $^{**}P < 0.01$, unpaired 2-tailed Student's t test. (**B**) $^{***}P < 0.001$, 1-way ANOVA followed by Newman-Keuls analysis.

administration promoted the restoration of cardiac function and morphology after MI, suggesting that MFG-E8 is a new therapeutic target for the treatment of MI.

Results

Cardiac myofibroblasts efficiently engulf dead cells. In the infarcted area after MI, many dead cells are rapidly generated. We considered that the recruited inflammatory cells are not sufficient for the removal of dead cells. Therefore, we hypothesized that myofibroblasts can engulf dead cells following MI in cooperation with macrophages. To test this hypothesis, we examined whether cardiac myofibroblasts isolated from infarcted hearts can engulf apoptotic cells ex vivo. We performed permanent occlusion of the left anterior descending artery to induce MI and isolated cardiac macrophages (Supplemental Figure 1A; supplemental material available online with this article; doi:10.1172/JCI83822DS1) (17) and myofibroblasts from mouse hearts 3 days after infarction. The lack of surface-marker protein specific for myofibroblasts led us to establish a method to selectively collect myofibroblasts from the infarcted hearts. Specifically, the infarcted mouse hearts were digested by collagenase/trypsin, and the digested cardiac cells were allowed to attach to the plates overnight. The attached cells included macrophages and myofibroblasts (positive for α smooth muscle actin [αSMA]) as well as other cardiac cells (Supplemental Figure 1B). Notably, cardiac myofibroblasts seemed to be more difficult than cardiac macrophages to collect using our isolation method from infarcted hearts because, as revealed by our immunohistochemical analysis, the number of cardiac myofibroblasts was the same as that of cardiac macrophages in the infarcted area (Supplemental Figure 1C). When the overnight-attached cells were cultured in 10% FBS/DMEM for more than 6 days, almost all of the cells on the plates were positive for αSMA and SM22α, 2 myofibroblast marker proteins (18, 19) (>97.9% and >93.8%, respectively) (Supplemental Figure 1, D and E), indicating that the cells were primarily composed of cardiac myofibroblasts. This is probably because only myofibroblasts were able to grow rapidly in the culture medium.

Isolated cardiac macrophages and myofibroblasts were allowed to engulf fluorescently labeled apoptotic cells, and we assessed the fluorescence taken up by cardiac macrophages and

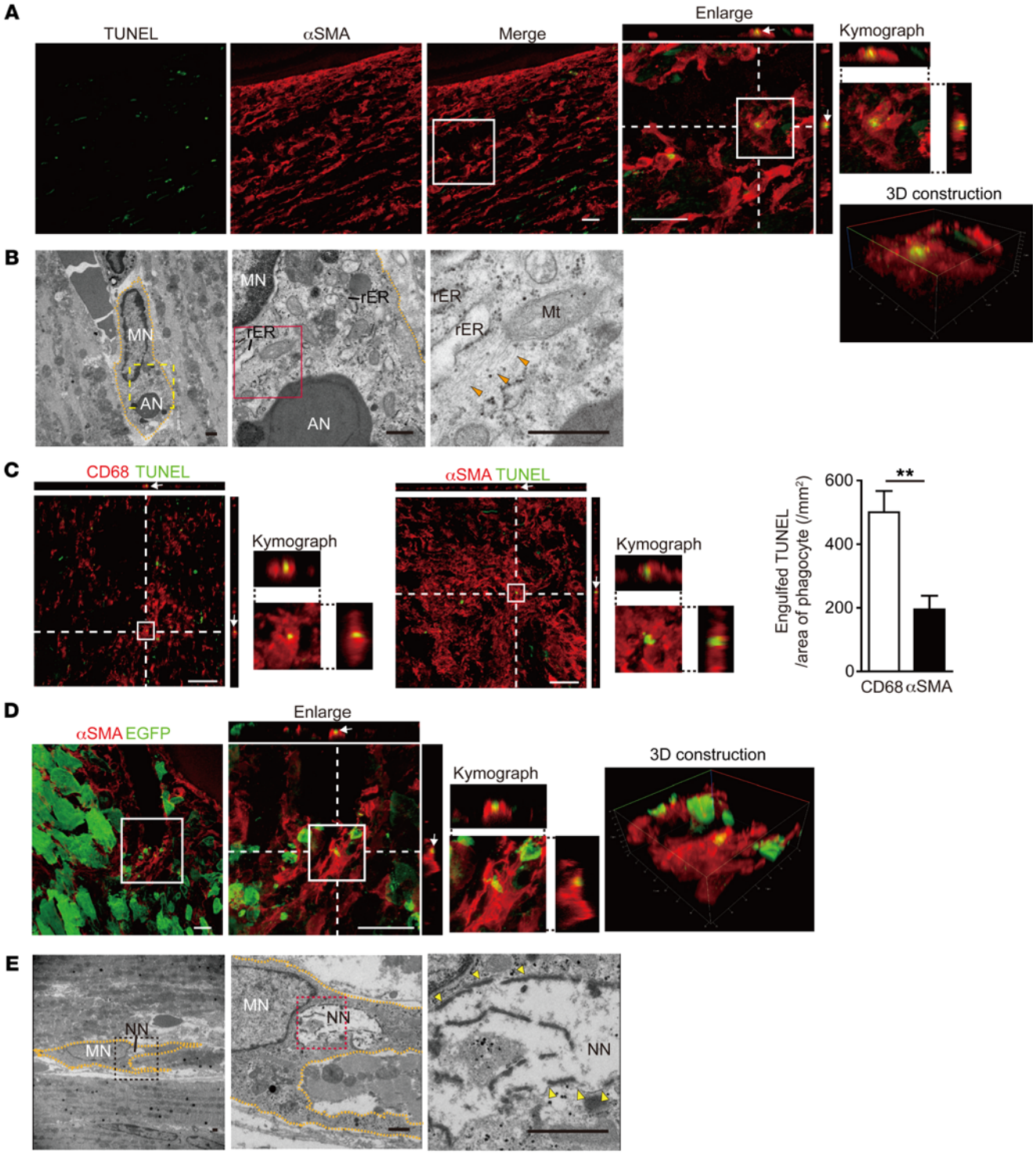

Figure 2. Cardiac myofibroblasts engulf dead cells in vivo. (**A**) Representative LV sections from WT mice that underwent MI were double stained with TUNEL (green) and anti-αSMA antibody (red) ($n = 4$). The area indicated by a white square on the merged image is enlarged. Kymograph along the white dashed line in the enlarged image is shown. The area indicated by a white square on the enlarged image was further enlarged, and a 3D image in a white square on the enlarged image is shown. White arrows indicate myofibroblasts containing an apoptotic cell. Scale bars: 30 μm. (**B**) Transmission electron micrographs of engulfment of an apoptotic cell by a myofibroblast. The areas in yellow and red boxes within a myofibroblast (orange dotted line) are enlarged in the middle and right panels. Well-developed rough-surfaced endoplasmic reticulum and intracellular actin filaments (arrowheads) can be seen in the myofibroblast. MN, myofibroblast nucleus; AN apoptotic nucleus; rER, rough-surfaced endoplasmic reticulum; Mt, mitochondria. Scale bar: 1 μm. (**C**) Quantification of engulfed TUNEL$^+$ apoptotic cells by macrophages (CD68$^+$) or myofibroblasts (αSMA$^+$) on the sections from mouse hearts 3 days after MI ($n = 4$). The number of engulfed apoptotic cells per square millimeter of CD68$^+$ macrophage or αSMA$^+$ myofibroblast area is shown. Scale bars: 50 μm. (**D**) Representative infarcted LV sections from WT mice with EGFP-labeled cardiomyocytes were stained with anti-αSMA antibody (red) ($n = 4$). Scale bars: 30 μm. (**E**) Transmission electron micrographs of engulfment of a necrotic cell by a myofibroblast. The areas in black and red dotted boxes are enlarged in middle and right panels. Necrotic nucleus (NN) was observed in the myofibroblast. Arrowheads indicate single-membrane structure. Scale bar: 1 μm. Error bars represent the mean ± SEM. (**C**) $^{**}P < 0.01$, unpaired 2-tailed Student's t test.

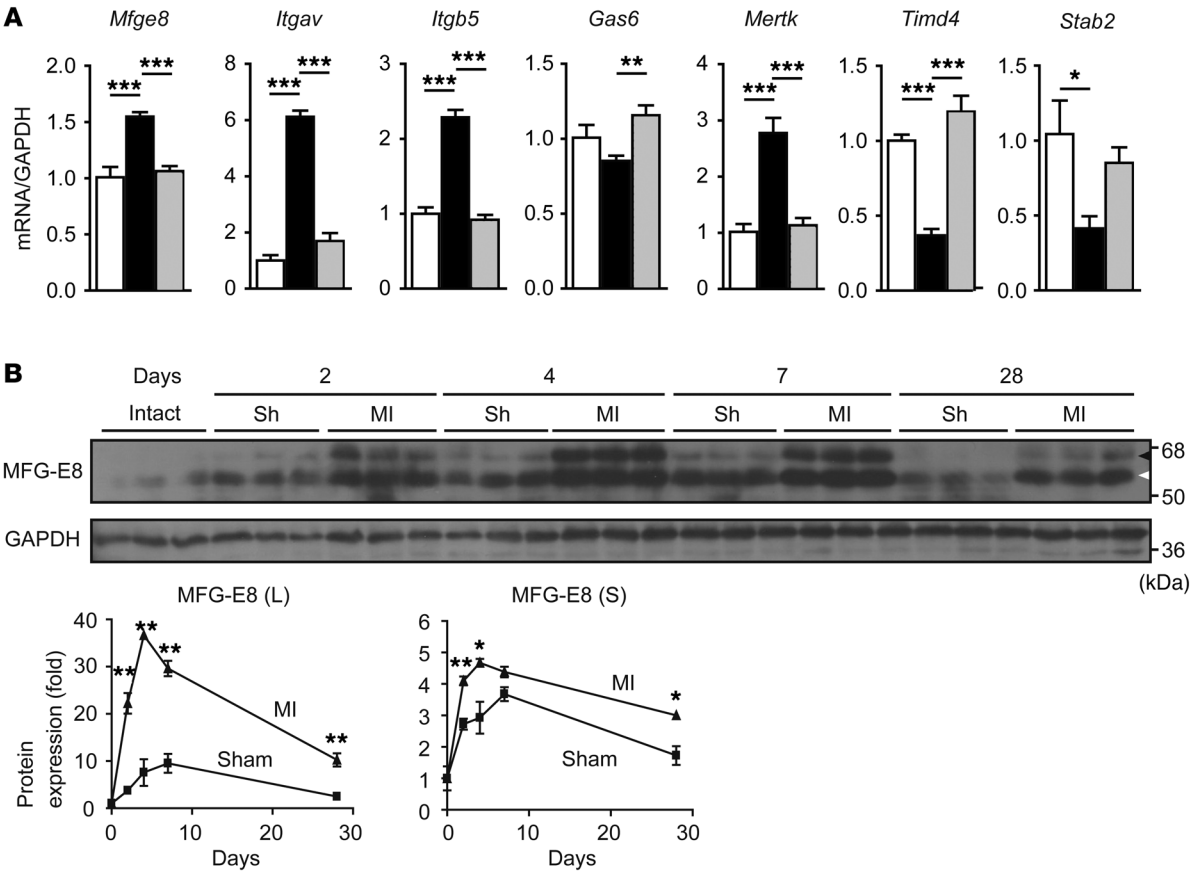

Figure 3. MFG-E8 expression is increased in the heart after MI. (**A**) mRNA expression levels of apoptotic cell recognition–related genes in hearts of sham-operated mice (white bars, $n = 3$) and in infarcted (black bars, $n = 5$) or remote areas (gray bars, $n = 5$) of mouse hearts 3 days after MI. (**B**) Western blot images of the long (black arrowhead) or short (white arrowhead) form of MFG-E8 in LV after sham (Sh) operation or MI. Western blot data were quantified ($n = 3$). Error bars represent the mean ± SEM. (**A**) $^*P < 0.05$; $^{**}P < 0.01$; $^{***}P < 0.001$, 1-way ANOVA followed by Newman-Keuls analysis. (**B**) $^*P < 0.05$; $^{**}P < 0.01$, unpaired 2-tailed Student's *t* test.

myofibroblasts. As previously reported (20), when phagocytes engulfed apoptotic cells, the apoptotic cells underwent a phase-bright to phase-dark transition. We also used this transition to distinguish engulfed apoptotic cells from those attached to phagocytes (Supplemental Figure 2A). Indeed, nearly all of the phase-dark apoptotic cells labeled with pH-sensitive pHrodo dyes — which are fluorescent only in acidic environments — exhibited fluorescence, indicating that these cells were internalized and fused with lysosomes (acidic organelles) in phagocytes (Supplemental Figure 2B). The fluorescence uptake and phase-bright to phase-dark transition revealed that cardiac macrophages effectively engulf apoptotic cells and, importantly, cardiac myofibroblasts also phagocytosed apoptotic cells. The engulfment ability of cardiac fibroblasts was about two-thirds of that of cardiac macrophages (Figure 1A). In addition, engulfment assays, which were performed for 6, 12, 18, and 24 hours, revealed that about 80% of the isolated cardiac myofibroblasts had the capacity to engulf dead cells (Supplemental Figure 2C).

Necrotic and necroptotic cells were detected in addition to apoptotic cells in the infarcted area (4, 5, 21). We determined whether myofibroblasts engulf necrotic cells ex vivo. Fluorescently labeled L929 cells that underwent necroptosis (22) were used as prey in the engulfment assay. Fluorescence signal was frequently localized in cardiac myofibroblasts, indicating that these cells also efficiently internalized necroptotic cells (Supplemental Figure 2D).

Cardiac myofibroblasts acquire antiinflammatory properties upon engulfment. Because cardiac myofibroblasts engulf dead cells in a manner similar to that of macrophages, we examined whether myofibroblasts had other engulfment-related properties characteristic of macrophages. It was reported that inflammatory cytokine production (e.g., IL-6) in macrophages is reduced after the engulfment of apoptotic cells, whereas anti-inflammatory cytokine production (e.g., TGF-β) in macrophages is increased (23). We found that the production of IL-6 (encoded by *Il6*) induced by LPS treatment in myofibroblasts was significantly attenuated by the engulfment of apoptotic cells (Figure 1B), whereas the LPS–induced production of TGF-β (encoded by *Tgfb1*) was increased following engulfment (Figure 1B). These results suggested that myofibroblasts attenuated inflammation in the infarcted area in a manner similar to that of macrophages and acquired antiinflammatory properties. We then costained the cardiac myofibroblasts with antibodies against CD45 — a hematopoietic marker — and αSMA to determine whether these cardiac myofibroblasts have a hematopoietic origin, similar to macrophages. The costaining revealed that the cardiac myofi-

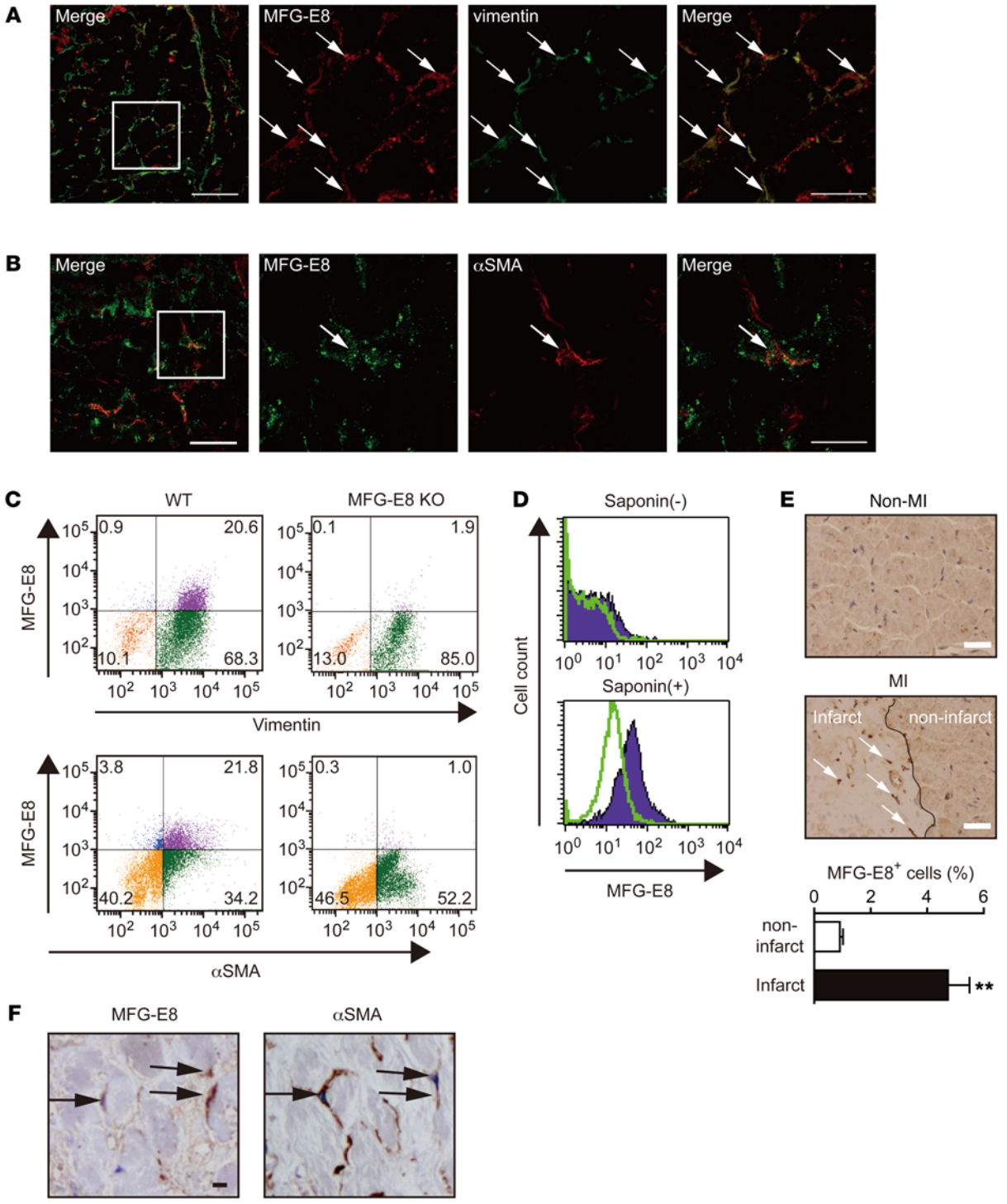

Figure 4. MFG-E8 is expressed in cardiac myofibroblasts after MI. (**A** and **B**) MFG-E8 expression colocalizes with vimentin-positive (**A**) or αSMA-positive (**B**) myofibroblasts in LV 3 days after MI (n = 4). White squares on merged images mark the magnified areas. Arrows indicate merged cells. Scale bars: 50 μm (lower magnification); 20 μm (higher magnification). (**C**) Cardiac myofibroblasts from WT or MFG-E8 KO mice were costained with anti–MFG-E8 and anti-vimentin or anti-αSMA antibodies (n = 4). Numbers in quadrants indicate the percentages of cells. (**D**) Cardiac myofibroblasts were stained with anti–MFG-E8 antibody without (–) or with saponin (+) permeabilization (n = 3). The staining profile (purple) and its control (without primary antibody; green) are shown. (**E**) Staining of heart sections from non-MI patients and patients with MI by anti–MFG-E8 antibody (n = 4). Arrows indicate MFG-E8 signals. Percentages of MFG-E8–positive cells in each area are shown in the graph. Scale bars: 30 μm. (**F**) Serial heart sections of patients with MI stained with anti–MFG-E8 antibody or anti-αSMA antibody. Arrows indicate double-positive myofibroblasts. Scale bar: 10 μm. Error bars represent the mean ± SEM. (**E**) $^{**}P < 0.01$, unpaired 2-tailed Student's t test.

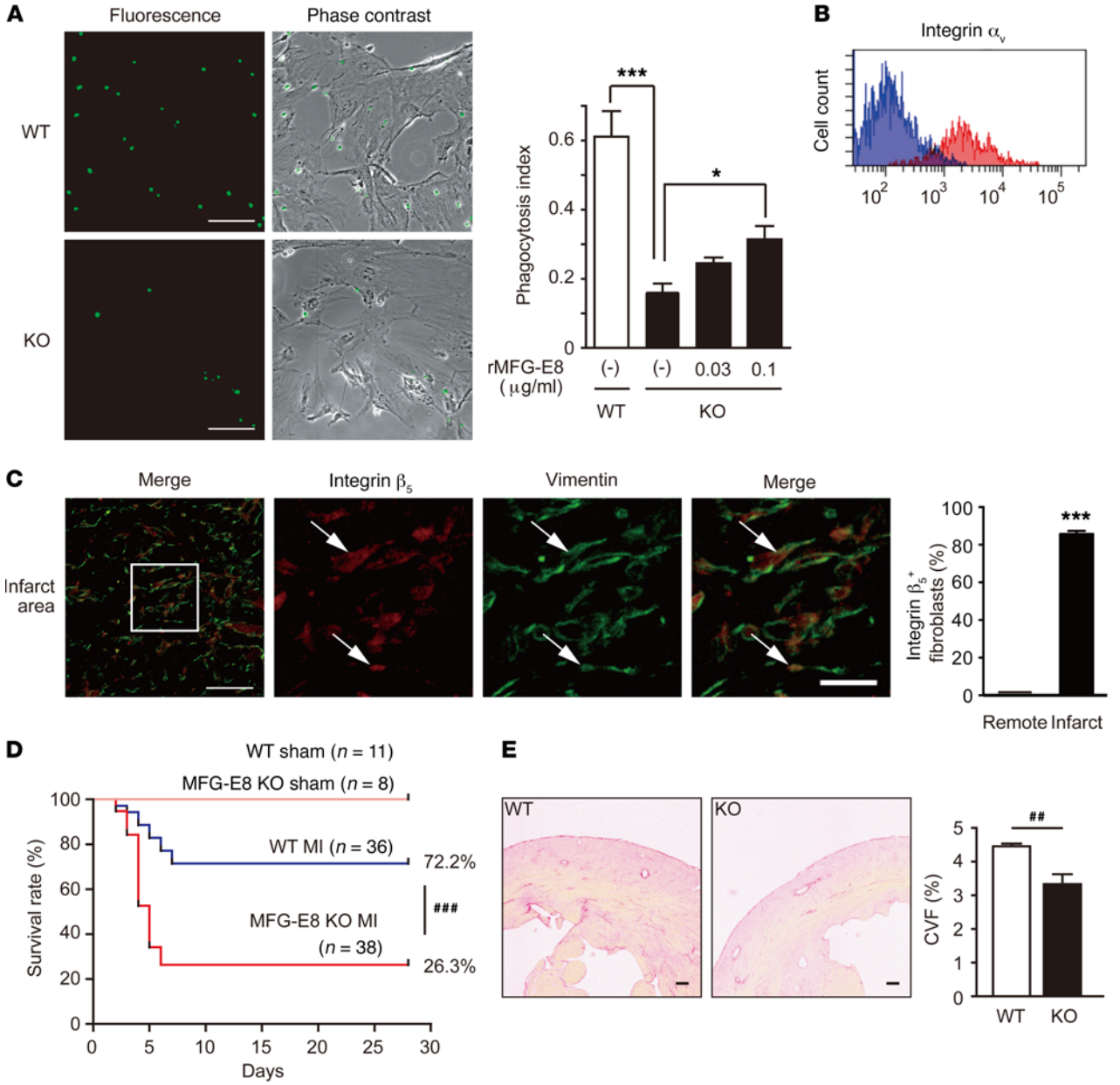

Figure 5. MFG-E8–dependent engulfment by cardiac myofibroblasts has a protective effect on heart after MI. (**A**) Cardiac myofibroblasts from WT and MFG-E8 KO mice were exposed to fluorescently labeled apoptotic cells in the absence (-) or presence of recombinant MFG-E8 (rMFG-E8). The number of engulfed apoptotic cells per myofibroblast was determined ($n = 4$). Scale bars: 100 μm. (**B**) The staining profile of cardiac myofibroblasts with PE–anti-integrin α_v antibody is shown in red ($n = 3$). The blue histogram represents the control. (**C**) Integrin β_5 (red) and vimentin (green) staining of infarcted area of heart sections from WT mice 3 days after MI ($n = 3$). A square on the first column marks the areas shown at a higher magnification. White arrows indicate vimentin-positive myofibroblasts merged with integrin β_5. The percentages of integrin β_5–positive fibroblasts in remote or infarct area of hearts after MI is shown in the graph. Scale bars: 50 μm (lower magnification); 20 μm (higher magnification). (**D**) Decreased survival rate of MFG-E8 KO mice (sham, $n = 8$; MI, $n = 38$) compared with that of WT mice (sham, $n = 11$; MI, $n = 36$) after MI. Kaplan-Meier survival analysis using a log-rank test. $^{###}P < 0.001$. (**E**) PicroSirius red staining of the cardiac sections of WT and MFG-E8 KO mice at day 3 after MI. The collagen volume fraction (CVF) was determined by counting collagen-depositing areas (WT, $n = 4$; KO, $n = 5$). Scale bars: 100 μm. Error bars represent the mean ± SEM. (**A**) $^{*}P < 0.05$; $^{***}P < 0.001$, 1-way ANOVA followed by Newman-Keuls analysis. (**C** and **E**) $^{***}P < 0.001$; $^{##}P < 0.01$, unpaired 2-tailed Student's t test.

broblasts did not express CD45 (Figure 1C), although we could not exclude the possibility that the cardiac myofibroblasts lost CD45 expression after differentiation. We also confirmed that these cardiac myofibroblasts do not express MHC class II (Supplemental Figure 3), ruling out the possibility that they function as antigen-presenting cells.

Cardiac myofibroblasts efficiently engulf apoptotic cells in vivo. We then examined whether cardiac myofibroblasts engulf apoptotic cells in vivo. Heart sections were prepared from mice 3 days after MI and double stained with TUNEL (green) and an antibody against αSMA (red). In this double staining, unengulfed apoptotic cells display green fluorescence, but when apoptotic cells are

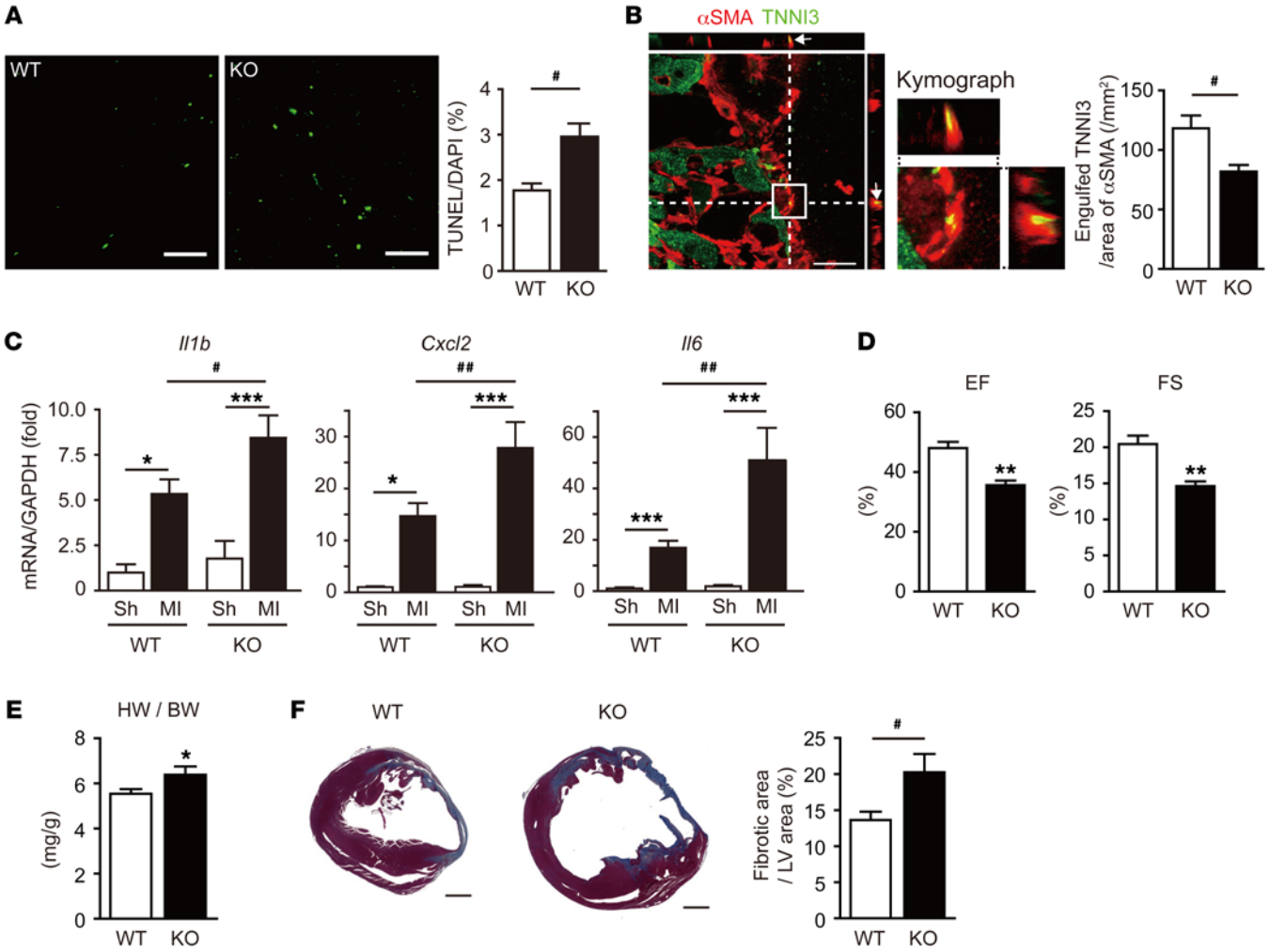

Figure 6. MFG-E8–dependent engulfment by cardiac myofibroblasts influences the conditions of heart after MI. (**A**) TUNEL-positive nuclei in the border zone of hearts in WT (n = 4) and MFG-E8 KO (n = 3) mice at day 3 after MI. The percentages indicate the ratio of TUNEL-positive nuclei to DAPI-positive nuclei. Scale bars: 100 μm. (**B**) Representative LV sections from WT mice that underwent MI were double-stained with anti-TNNI3 (green) and anti-αSMA (red) antibodies (n = 5). The numbers of TNNI3-positive cardiomyocytes per square millimeter of αSMA-positive area in infarcted hearts of WT and MFG-E8 KO mice are shown in the graph. Scale bar: 20 μm. (**C**) mRNA expression levels of inflammatory genes 3 days after sham operation or MI in the hearts of WT or MFG-E8 KO mice (sham, n = 4; MI, n = 5). (**D**) Echocardiographic measurements of WT mice (n = 7) or MFG-E8 KO mice (n = 5) at 4 weeks after MI. Ejection fraction (EF) and fractional shortening (FS) are shown. (**E**) Ratio of heart weight (HW) to body weight (BW) of WT mice (n = 7) or MFG-E8 KO mice (n = 5) at 4 weeks after MI. (**F**) Representative heart sections of WT mice (n = 6) or MFG-E8 KO mice (n = 5) at 4 weeks after MI stained with Masson's trichrome. The ratios of the fibrotic area to the LV area were quantitatively estimated and are shown in the graph. Scale bars: 1 mm. Error bars represent the mean ± SEM. (**A**, **B**, **D**–**F**) $^*P < 0.05$; $^{**}P < 0.01$; $^{\#}P < 0.05$, unpaired 2-tailed Student's t test. (**C**) $^*P < 0.05$; $^{***}P < 0.001$; $^{\#}P < 0.05$; $^{\#\#}P < 0.01$, 1-way ANOVA followed by Newman-Keuls analysis.

engulfed, they appear yellow as an overlay of green and red (24–26). Confocal microscopy showed yellow signal inside αSMA-positive cells at the infarct and border areas of infarcted hearts, suggesting that cardiac myofibroblasts engulfed apoptotic cells in these areas (Figure 2A). However, TUNEL- or αSMA-positive signals were rarely observed in remote areas of infarcted hearts (Supplemental Figure 4).

To confirm that cardiac myofibroblasts engulf apoptotic cells in vivo, we examined myofibroblasts in infarcted mouse heart tissue sections by electron microscopy. Myofibroblasts are characterized by a well-developed rough endoplasmic reticulum and intracellular actin filaments (27). Many myofibroblasts were detected in the infarcted area, some of which had internalized an apoptotic nucleus (Figure 2B). These results indicated that cardiac myofibroblasts take up apoptotic cells.

We then compared the contributions of cardiac myofibroblasts and cardiac macrophages to the clearance of dead cells in MI. As shown in Supplemental Figure 1C, the number of cardiac myofibroblasts was almost the same as the number of cardiac macrophages in the infarcted area. TUNEL-positive signals in cardiac macrophages (CD68-positive cells) or myofibroblasts (αSMA-positive cells) in the infarcted area were counted, and we found that the number of apoptotic cells engulfed by myofibroblasts in the infarcted hearts was about 40% of that engulfed by macrophages (Figure 2C). These data suggested that the contribution of cardiac myofibroblasts for engulfment was about two-fifths that of cardiac macrophages (Figure 2C).

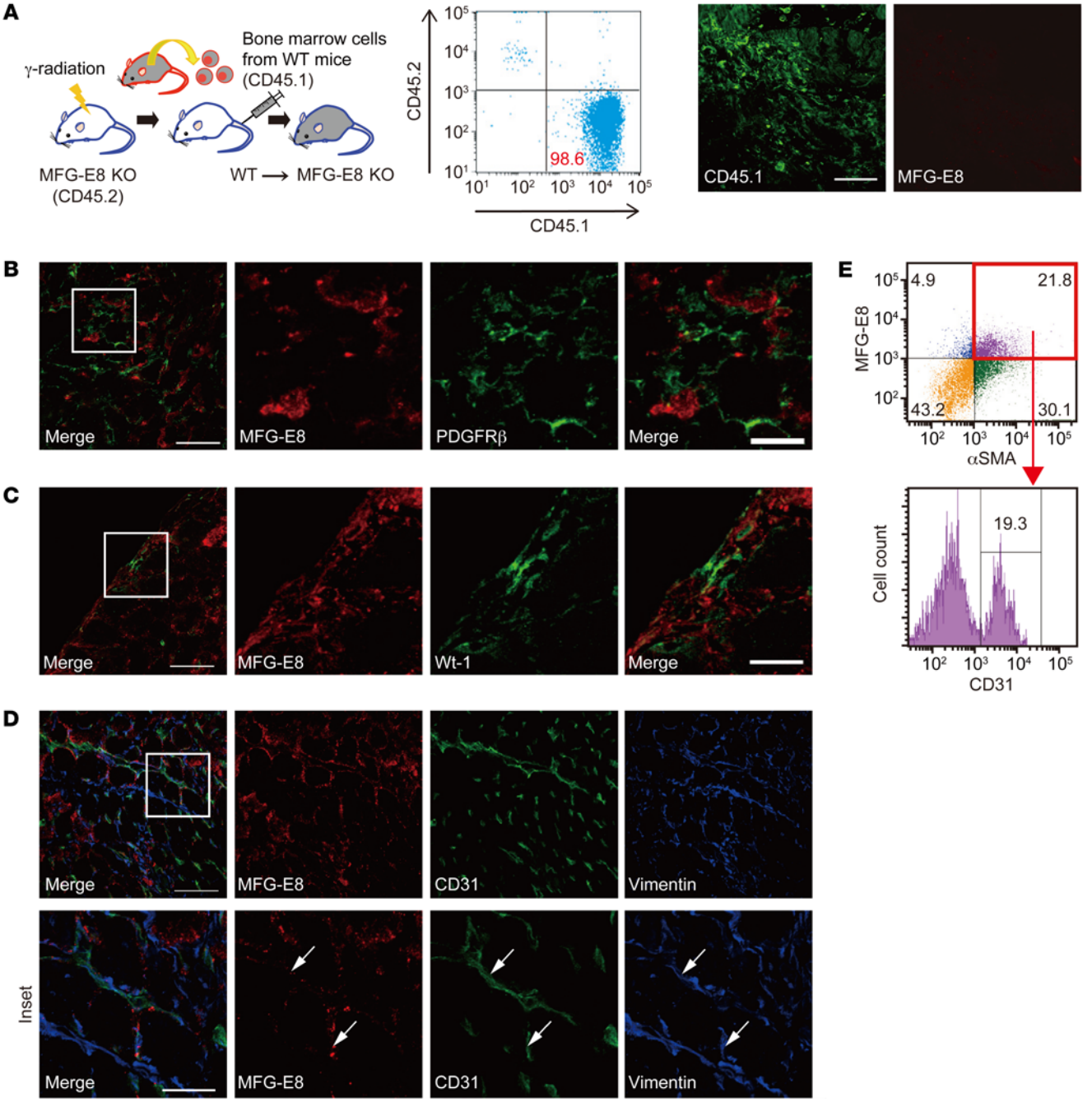

Figure 7. MFG-E8 is produced in myofibroblasts derived from resident cardiac fibroblasts or cells that underwent EndMT. (**A**) Schematic representation of the experimental design. LV sections from infarcted MFG-E8 KO mice (CD45.2$^+$) transplanted with the bone marrow cells of WT mice (CD45.1$^+$) were stained with anti-CD45.1 (green) and anti–MFG-E8 (red) antibodies (n = 3). Scale bar: 50 μm. FACS dot plot of peripheral blood cells for recipient-type CD45.2-APC and donor-type CD45.1-FITC is shown. (**B** and **C**) LV sections from WT mice on day 3 after MI were stained with anti–MFG-E8 (red) and anti-PDGFRβ (green) (**B**) or anti–MFG-E8 (red) and anti–Wt-1 (green) (**C**) antibodies (n = 3). White squares on the merged images (first columns) mark the areas shown at a higher magnification. Higher-magnification images are shown on the right side of lower-magnification images. Scale bars: 50 μm (lower magnification); 20 μm (higher magnification). (**D**) LV sections from WT mice on day 3 after MI were stained with anti–MFG-E8 (red), anti-CD31 (green), and anti-vimentin (blue) antibodies. The first column is the merged image of MFG-E8, CD31, and vimentin. The magnified views of the white boxed region on the low-magnification merged images are displayed in a vertical row. The insets (lower panels) show the details of the MFG-E8, vimentin, and CD31 immunoreactive myofibroblasts. Scale bars: 50 μm (lower magnification); 20 μm (higher magnification). White arrows indicate merged cells. (**E**) Cardiac myofibroblasts isolated from WT mice on day 3 after MI were stained with anti–MFG-E8, FITC-anti-αSMA, and PerCP/Cy5.5-anti-CD31 antibodies and analyzed by flow cytometry (n = 4). Representative data are shown (**A**–**E**).

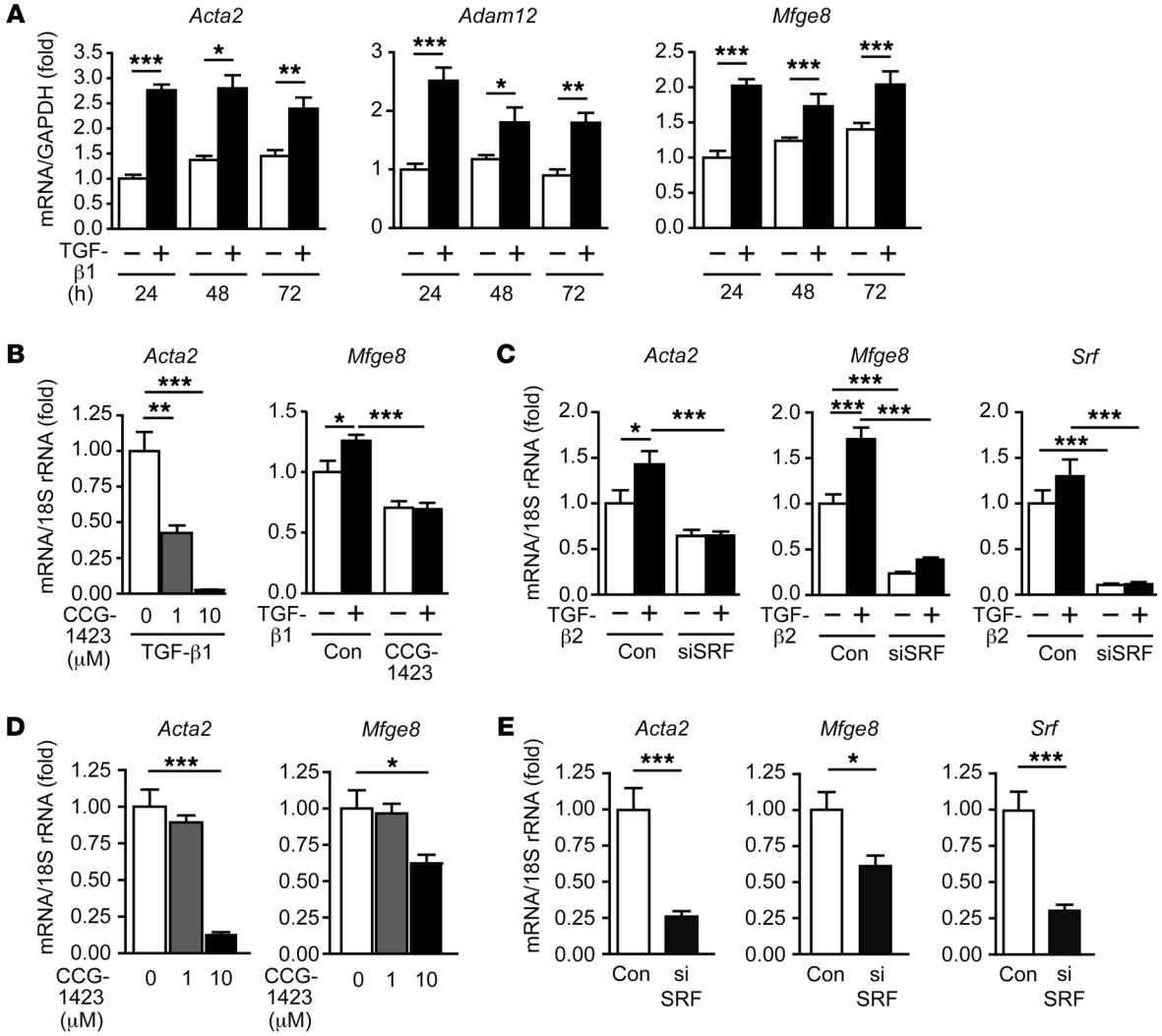

Figure 8. MFG-E8 is produced in myofibroblasts via the SRF-dependent pathway. (**A**) *Acta2*, *Adam12*, and *Mfge8* mRNA expression levels in rat neonatal cardiac fibroblasts treated with TGF-β1 (24, 48, and 72 hours, $n = 5$). (**B**) *Acta2* and *Mfge8* mRNA expression levels in rat neonatal cardiac fibroblasts treated with TGF-β1 (10 ng/ml) in the absence or presence of CCG-1423 (1 or 10 μM, $n = 5$ or 6). (**C**) *Acta2*, *Mfge8*, and *Srf* mRNA expression levels in HUVECs treated with or without TGF-β2 (10 ng/ml) for 72 hours in the presence of siRNA against SRF ($n = 4$ or 5). (**D** and **E**) *Acta2* and *Mfge8* mRNA expression levels in cardiac myofibroblasts, which were treated with or without CCG-1423 (1 or 10 μM) for 24 hours (**D**) or treated with siRNA against SRF (**E**) ($n = 4$ or 5). Decreased *Srf* mRNA expression in myofibroblasts treated with siRNA against SRF was confirmed in **E** ($n = 4$ or 5). Error bars represent the mean ± SEM. (**A–D**) $^*P < 0.05$; $^{**}P < 0.01$; $^{***}P < 0.001$, 1-way ANOVA followed by Newman-Keuls analysis. (**E**) $^*P < 0.05$; $^{***}P < 0.001$, unpaired 2-tailed Student's *t* test.

To determine the identity of cells engulfed by myofibroblasts, we specifically labeled cardiomyocytes with EGFP using the adeno-associated virus 9 (AAV9) vector system with the cardiac troponin T (cTnT) promoter to drive cardiomyocyte-specific expression (28, 29) (Supplemental Figure 5, A and B). Confocal microscopy showed that αSMA-positive cells were located in the border areas of infarcted mouse hearts (Figure 2D), but not in remote areas (Supplemental Figure 5B). Furthermore, some EGFP signal was detected inside αSMA-positive cells (Figure 2D), demonstrating that myofibroblasts engulf dead cardiomyocytes in MI. This was confirmed by FACS analysis; in the intact mouse heart, platelet-derived growth factor receptor-α–positive (PDGFR-α–positive) cells were negative for EGFP (Supplemental Figure 5, C and D). However, 3 days after MI, a fraction of PDGFR-α–positive cells — most of which were presumed to be myofibroblasts — expressed EGFP (Supplemental Figure 5, C and D).

We next investigated whether necrotic cardiomyocytes are engulfed by myofibroblasts in vivo. Electron microscopy revealed that myofibroblasts in the infarcted area contained a degraded nucleus (Figure 2E), presumably derived from necrotic cardiomyocytes that were abundant in the infarcted area (Supplemental Figure 6A). The phagosome-containing degraded nucleus was a single-membrane structure of about 4 μm, indicating that the phagosome was different from autophagosome and autolysosome in mammalian cells (0.5–1.5 μm) (30). We also investigated whether necroptotic cardiomyocytes are engulfed by myofibroblasts in vivo. Cardiomyocytes were infected with EGFP fused with receptor-interacting protein 3 (RIP3), which plays an important role in promoting necroptosis (31). RIP3 overexpression increases the probability of necroptosis in cardiomyocytes (32). In infarcted hearts of mice with cardiomyocytes labeled with RIP3-EGFP,

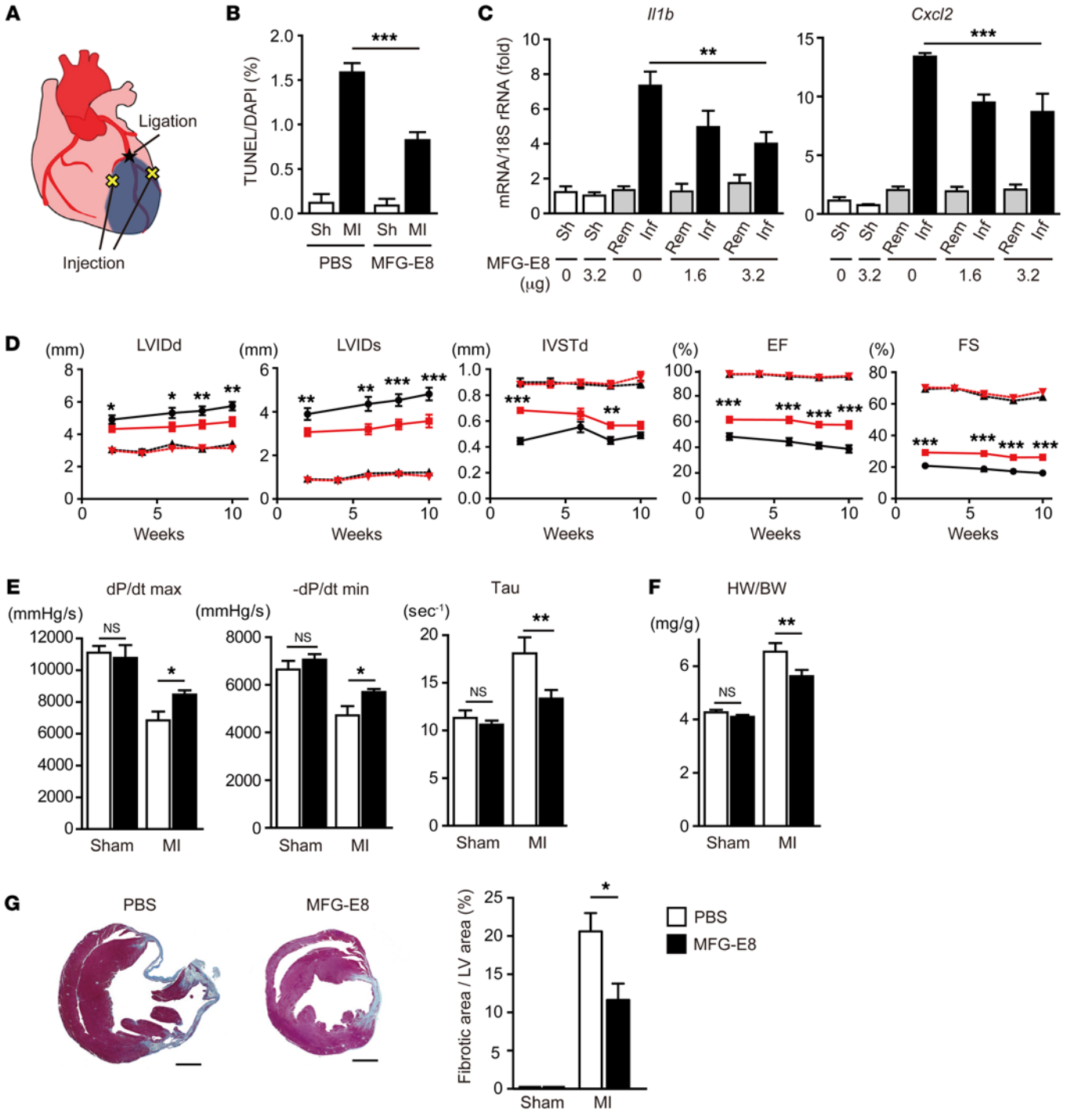

Figure 9. MFG-E8 administration after MI improves cardiac function in vivo. (**A**) Schematic representation of MFG-E8 intramyocardial injection. (**B**) TUNEL-positive nuclei in border zone of PBS- or MFG-E8–administered mice (3.2 μg) (sham, $n = 5$; MI, $n = 7$) 3 days after MI. (**C**) MFG-E8 intramyocardial injection (1.6 or 3.2 μg) decreased expression of the upregulated inflammatory genes at the infarct (Inf), not remote (Rem), areas of hearts 3 days after MI ($n = 4$ each). (**D**) Temporal changes in echocardiographic parameters (LV end-diastolic internal diameter [LVIDd], LV end-systolic internal diameter [LVIDs], interventricular-septal thickness at end-diastole [IVSTd], ejection fraction, and fractional shortening) of PBS-treated (sham, $n = 7$, black-dotted lines; MI, $n = 10$, black lines) or MFG-E8–treated mice (sham, $n = 7$, red-dotted lines; MI; $n = 7$, red lines) 2, 6, 8, and 10 weeks after MI. (**E**) Hemodynamic parameters (dP/dtmax, -dP/dtmin, and Tau) of PBS-treated (sham, $n = 3$; MI, $n = 7$) or MFG-E8–treated mice (sham, $n = 5$; MI, $n = 7$) 10 weeks after MI. (**F**) Heart weight to body weight ratio of PBS-treated (sham, $n = 7$; MI, $n = 10$) or MFG-E8–treated mice (sham, $n = 7$; MI, $n = 9$) 10 weeks after MI. (**G**) Representative Masson's trichrome–stained heart sections of PBS-administered ($n = 6$) or MFG-E8–administered mice ($n = 5$) 10 weeks after MI. Scale bars: 1 mm. Error bars represent the mean ± SEM. $^*P < 0.05$; $^{**}P < 0.01$; $^{***}P < 0.001$, 1-way ANOVA followed by Newman-Keuls analysis.

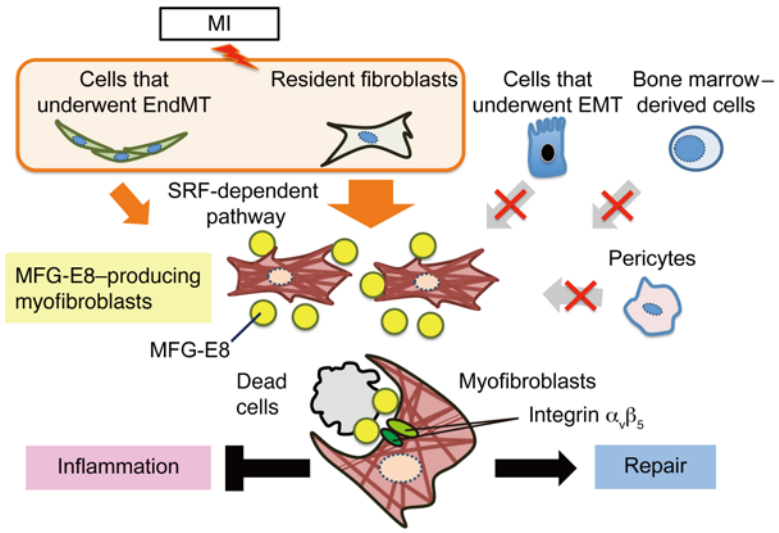

Figure 10. Schematic model depicting origins and functions of MFG-E8–producing myofibroblasts appearing at the infarcted area after MI. Resident fibroblasts and cells that underwent EndMT differentiate into MFG-E8–producing myofibroblasts upon inflammation. MFG-E8 was produced during the differentiation via the SRF-dependent pathway. The myofibroblasts not only produce extracellular matrix, but also engulf dead cells via an MFG-E8/integrin $\alpha_v\beta_5$–dependent pathway, and attenuate inflammation, similarly to macrophages.

we observed EGFP fluorescence inside αSMA-positive cells at the border areas, suggesting that necroptotic cardiomyocytes were engulfed by cardiac myofibroblasts (Supplemental Figure 6B). These results provide in vivo evidence that myofibroblasts engulf apoptotic and necrotic cardiomyocytes in MI.

MFG-E8 is upregulated in hearts after MI. To identify the molecules involved in the engulfment of dead cells by cardiac myofibroblasts after MI, we examined mRNA expression of several molecules that are involved in the recognition of apoptotic cells (7) in the infarcted area. Three days after MI, infarcted mouse hearts were surgically removed and subdivided into "infarcted areas" and "non-infarct remote areas." RNA from each area was isolated. Real-time reverse-transcription PCR (RT-PCR) analysis revealed that mRNA levels of *Mfge8*, a secreted protein that promotes engulfment (15, 16), and its corresponding receptor on phagocytes, integrin receptor $\alpha_v\beta_5$ (*Itgav*, *Itgb5*) (15), were both increased in the infarcted areas, but not in the remote areas (Figure 3A). MER (*Mertk*), a phagocytic receptor that recognizes apoptotic cells via GAS6, was also induced selectively in infarcted areas after occlusion (Figure 3A), whereas *Gas6* expression was not increased. Conversely, the expression of TIM4 (*Timd4*) and stabilin 2 (*Stab2*) was decreased in the infarcted area (Figure 3A). BAI-1, another phagocytic receptor, was not detected in either intact or infarcted hearts.

Among the molecules selectively upregulated in infarcted areas, Mer was recently reported to be expressed in macrophages that infiltrate the infarcted area and mediate the removal of dead cells (8). Thus, we focused on the MFG-E8/integrin $\alpha_v\beta_5$ pathway of engulfment. Consistent with the RT-PCR result, the protein levels of 2 isoforms of MFG-E8 (long and short forms) (16) greatly increased, peaking 4 days after MI surgery, and then gradually decreased (Figure 3B). These results prompted us to investigate whether MFG-E8 mediates engulfment by cardiac myofibroblasts.

MFG-E8 expression is induced in myofibroblasts after MI in mice and humans. We examined whether cardiac myofibroblasts express MFG-E8 after MI in the heart. Immunohistochemical staining of heart sections with an antibody against MFG-E8 at 1 or 3 days after occlusion revealed that MFG-E8–positive cells were mainly found in the infarct and border areas where abundant cell death had occurred (Supplemental Figure 7, A–C). The infarct areas were characterized by sparse DAPI signal (Supplemental Figure 7A–C). In contrast, MFG-E8–positive cells were not detected in remote areas where few dead cells were generated (Supplemental Figure 7, A–C). Myofibroblasts are characterized by vimentin (pan-fibroblast marker, fibroblast and myofibroblast marker) and αSMA expression (19). Immunohistochemical staining revealed that vimentin- and αSMA-immunoreactive cells exhibited positive immunostaining for MFG-E8, implying that myofibroblasts produce MFG-E8 (Figure 4, A and B). Consistent with these results, isolated cardiac myofibroblasts were positive for MFG-E8 (Supplemental Figure 7D). In contrast, inflammatory cells recruited to infarcted areas (i.e., infarct and border areas), including CD68-positive macrophages (Supplemental Figure 8A) and Gr-1–positive neutrophils (Supplemental Figure 8B) as well as α-actinin–positive cardiomyocytes (Supplemental Figure 8C), did not exhibit MFG-E8 immunoreactivity.

A previous report demonstrated that MFG-E8–positive signals can be detected via immunohistochemical analysis of splenic macrophages that do not produce MFG-E8 by themselves, as MFG-E8 secreted from follicular dendritic cells is trapped by integrin receptors on the macrophages (25). Therefore, we stained the cells collected by our procedure to selectively collect fibroblasts (both resident fibroblasts and myofibroblasts) from infarcted hearts with anti–MFG-E8 antibody with or without saponin treatment. As shown in Figure 4C, nearly 90% (WT, 20.6% + 68.3% = 88.9%; MFG-E8 KO, 85.0% + 1.9% = 86.9%) of the collected cells isolated by the procedure were vimentin positive. We then coimmunostained the myofibroblasts isolated from WT and *Mfge8*$^{-/-}$ mice (herein referred to as MFG-E8 KO) with anti–MFG-E8 antibody in combination with anti-vimentin or anti-αSMA antibodies after saponin permeabilization and analyzed them using FACS. Cardiac myofibroblasts (αSMA-positive cells) made up approximately 55% (WT, 21.8% + 34.2% = 56.0%; MFG-E8 KO, 1.0% + 52.2% = 53.2%) of the collected cells, and 40% (WT, (21.8%/[21.8% + 34.2%]) × 100%) of the myofibroblasts were MFG-E8 positive (Figure 4C). MFG-E8–positive myofibroblasts were not detected when cardiac fibro-

blasts were isolated from MFG-E8 KO mice (Figure 4C). FACS analysis also revealed that isolated cardiac myofibroblasts were only stained with anti–MFG-E8 antibody after saponin treatment (Figure 4D), ruling out the possibility that MFG-E8 was trapped by integrin receptors. We also confirmed that MFG-E8–positive cells were negative for CD21/CD35, a typical follicular dendritic cell marker (33) (Supplemental Figure 8D). Consistently, immunohistochemical analysis demonstrated that CD21/CD35-positive cells were not found in the infarcted hearts (Supplemental Figure 8E). These results demonstrated that a portion of cardiac myofibroblasts produced MFG-E8 after MI.

We next examined whether MFG-E8–producing cells were observed in the hearts of patients with MI. MFG-E8–expressing cells selectively appeared in the interstitium of the infarcted area in MI patients (Figure 4E). We then examined whether these MFG-E8–positive cells are myofibroblasts. We used serial heart sections of patients with MI stained for MFG-E8 and αSMA staining. The staining revealed that MFG-E8–positive cells expressed αSMA (Figure 4F), suggesting that MFG-E8–producing myofibroblasts play a role in the pathogenesis of human MI.

Myofibroblasts engulf apoptotic cells via MFG-E8. We assessed the ability of myofibroblasts from WT and MFG-E8 KO mice to engulf apoptotic cells. We found that myofibroblasts from WT mice efficiently phagocytosed apoptotic cells, but myofibroblasts isolated from MFG-E8 KO mice exhibited severely decreased engulfment (Figure 5A). This diminished engulfment was recovered by MFG-E8 addition in a concentration-dependent manner (Figure 5A), demonstrating that engulfment by cardiac myofibroblasts depends on MFG-E8.

We then investigated whether cardiac myofibroblasts express integrin $\alpha_v\beta_5$, a receptor for MFG-E8. FACS analysis of cells stained with an antibody against integrin α_v revealed that the receptor was expressed in cardiac myofibroblasts (Figure 5B). Furthermore, immunohistochemical analysis demonstrated that most vimentin-positive signals in infarcted areas were found in integrin β_5-positive cells, indicating that myofibroblasts expressed integrin β_5 (Figure 5C). These cells were not detected in remote areas of infarcted hearts (Supplemental Figure 9). These results suggested that MFG-E8/integrin $\alpha_v\beta_5$ mediated engulfment by cardiac myofibroblasts.

Hyperinflammation caused by accumulation of dead cells after MI in MFG-E8 KO mice leads to deterioration of cardiac function and morphology. To investigate the physiological importance of engulfment by cardiac myofibroblasts via MFG-E8 in MI, we assessed the survival of WT and MFG-E8 KO mice after the infarction. In WT mice, the survival rate 28 days after MI was 72.2% ($n = 36$), but the rate in MFG-E8 KO mice ($n = 38$) was remarkably decreased to 26.3% (Figure 5D), indicating that MFG-E8 plays a critical role in the healing process after MI. Evans blue dye and 2,3,5-triphenyl tetrazolium chloride (TTC) staining of heart sections from WT and MFG-E8 KO mice 3 hours after MI revealed that the size of area at risk (AAR) and infarct area were similar between the 2 groups (Supplemental Figure 10A). H&E and PicroSirius red staining of heart sections revealed that wall thickening (Supplemental Figure 10B) and fibrosis (Figure 5E) were attenuated in MFG-E8 KO mice 3 days after MI, suggesting an increase of cardiac rupture after MI in the KOs. Consistent with these observations, the number of myofibroblasts (Supplemental Figure 10C) and the induction of actin alpha (*Acta2*), which encodes αSMA, and the genes encoding integrin $\alpha_v\beta_5$ at the infarcted area were reduced in MFG-E8 KO mice (Supplemental Figure 10D).

The difference in the survival rate between WT and MFG-E8 KO mice was evident during days 3–5 after MI (Figure 5D). We compared the condition of the WT versus MFG-E8 KO mouse hearts 3 days after infarction to explore the role of MFG-E8–mediated engulfment by cardiac myofibroblasts. We first performed a TUNEL assay of infarcted heart sections of WT and MFG-E8 KO mice to test for defects in apoptotic engulfment. The assay revealed that the number of TUNEL-positive cells was increased in the infarcted heart tissues of MFG-E8 KO mice (Figure 6A). Consistent with this result, the ability of cardiac myofibroblasts to engulf dead cardiomyocytes was decreased in MFG-E8 KO mice (Figure 6B and Supplemental Figure 11A). The addition of MFG-E8 to cardiomyocytes did not influence their death (Supplemental Figure 11B), suggesting that MFG-E8 does not contribute to cardiomyocyte cell death, as in the case of splenocytes (24). Unengulfed apoptotic cells undergo secondary necrosis, leading to the leakage of their intracellular contents and excessive inflammation (7). We then examined the expression levels of inflammatory genes in heart tissues of WT and MFG-E8 KO mice after MI. RT-PCR experiments demonstrated that the inflammatory genes *Il1b*, *Cxcl2*, *Tnf*, *Il6*, and *Mmp9* were upregulated by MI and that the upregulation was significantly higher in MFG-E8 KO mice (Figure 6C and Supplemental Figure 12A). However, the induction of antiinflammatory genes in the heart after MI was similar between WT and MFG-E8 KO mice (Supplemental Figure 12B). These results demonstrated that the accumulation of apoptotic cells and inflammatory responses after MI were augmented in the MFG-E8 KO mice due to a defect in engulfment by cardiac myofibroblasts.

Hyperinflammation of the infarcted area leads to deterioration of cardiac function after MI (5, 9). We therefore examined cardiac function, morphology, and infarct size 28 days after MI. Echocardiography and hemodynamic measurements demonstrated that cardiac function and morphology were deteriorated in MFG-E8 KO mice (Figure 6D and Supplemental Figure 13), while there was no difference between nonoperated WT and MFG-E8 KO mice in terms of cardiac function (Supplemental Table 1). In addition, heart weight and infarct area after MI were markedly increased in MFG-E8 KO relative to those in control mice (Figure 6, E and F).

MFG-E8–producing myofibroblasts are derived from resident fibroblasts and cells that have undergone EndMT. It has been reported that cardiac myofibroblasts are derived from the following 5 cell types during inflammation (14, 34): bone marrow–derived cells, pericytes, cells that have undergone EMT and EndMT, and resident fibroblasts. As shown in Figure 4C, 40% of cardiac myofibroblasts (αSMA-positive cells) were MFG-E8 positive 3 days after MI. This result indicates that MFG-E8 is a new determinant that functionally characterizes a subpopulation of myofibroblasts. Therefore, we sought to determine the origin of MFG-E8–producing myofibroblasts. We first examined whether bone marrow cells differentiated into MFG-E8–producing myofibroblasts. Bone marrow cells obtained from WT mice (CD45.1 allotype) were transplanted into lethally irradiated MFG-E8 KO mice (CD45.2 allotype), and 2 weeks after the transplantation, the engraftment efficiency of these cells in the mice was determined to be more

than 95% (Figure 7A). After MI, CD45.1-positive cells appeared in the infarcted area, but MFG-E8–positive myofibroblasts were not observed (Figure 7A). Further, to assess whether MFG-E8–producing myofibroblasts were derived from pericytes, infarcted heart sections were coimmunostained with antibodies against MFG-E8 and PDGFRβ (35). However, PDGFRβ failed to colocalize with MFG-E8 (Figure 7B). Furthermore, we tested to determine whether MFG-E8–producing myofibroblasts originated from cells that underwent EMT, identified by Wt1 expression (36, 37). As reported previously, myofibroblasts positive for Wt1 were found in the infarcted area (36), but these cells did not produce MFG-E8 (Figure 7C). In addition, the upregulation of other EMT markers — namely, T-box 18 (Tbx18) and Snai1 (37, 38) — in infarcted areas was comparable between WT and MFG-E8 KO mice, suggesting that MFG-E8 does not contribute to EMT (Supplemental Figure 14A). Cells expressing S100A4 (fibroblast-specific protein-1), a proposed marker for a subset of myofibroblasts (39), were similarly negative for MFG-E8 (Supplemental Figure 14B).

Conversely, triple immunohistochemical staining for CD31, a marker for myofibroblasts that underwent EndMT (39, 40), MFG-E8, and vimentin, revealed that some cells are triple positive, indicating that a portion of MFG-E8–producing myofibroblasts were derived from EndMT cells (CD31-positive) (Figure 7D). Consistently, FACS analysis of cardiac myofibroblasts using CD31, MFG-E8, and αSMA antibodies demonstrated that approximately 20% of MFG-E8–producing myofibroblasts were derived from EndMT cells (Figure 7E). Previous reports (14, 34) suggested that myofibroblasts that were not derived from bone marrow–derived cells, pericytes, or cells that underwent EMT or EndMT were generated from resident cardiac fibroblasts because a specific marker for myofibroblasts differentiated from resident fibroblasts has not yet been identified. Therefore, we reasoned that the remaining MFG-E8–positive myofibroblasts (approximately 80%) originated from resident cardiac fibroblasts. Taken together, these results suggested that MFG-E8–positive myofibroblasts were derived mainly from cardiac-resident fibroblasts and from cells that underwent EndMT.

MFG-E8 expression in myofibroblasts is induced by the SRF-dependent pathway. Despite the importance of MFG-E8 in apoptotic engulfment by macrophages (24, 25), the molecular machinery regulating MFG-E8 production in phagocytes has long been obscure. We set out to investigate the mechanism underlying MFG-E8 production by myofibroblasts. Resident cardiac fibroblasts were found to be the main source of MFG-E8–positive cardiac myofibroblasts. We thus examined whether MFG-E8 was induced in resident cardiac fibroblasts by TGF-β treatment, which transdifferentiates them into myofibroblasts (41, 42). Because it is difficult to acquire a sufficient number of resident cardiac fibroblasts from mice for in vitro experiments, we used a transdifferentiation system using rat neonatal resident cardiac fibroblasts (41). As reported previously (41), treatment of rat neonatal resident cardiac fibroblasts with TGF-β1 induced the expression of *Acta2*, which encodes αSMA, and a disintegrin and metalloproteinase 12 (ADAM12), another myofibroblast marker protein (43) (Figure 8A), indicating that the resident fibroblasts were transdifferentiated. In the TGF-β1–stimulated resident fibroblasts, *Mfge8* expression was induced (Figure 8A) with a time course similar to those of *Acta2* and *Adam12* (Figure 8A). Because *Acta2* expression induced by TGF-β treatment was reported to depend on SRF (41, 44), we examined whether SRF is also involved in MFG-E8 production. RT-PCR analysis demonstrated that pretreatment of resident fibroblasts with CCG-1423 (45), an inhibitor of SRF, attenuated *Acta2* expression induced by TGF-β1 in a concentration-dependent manner (Figure 8B). Similar to *Acta2* expression, TGF-β–induced *Mfge8* expression was significantly attenuated by CCG-1423 treatment in resident cardiac fibroblast (Figure 8B), suggesting that SRF mediated TGF-β–induced *Mfge8* expression in these cells.

We further examined whether MFG-E8 was also induced in EndMT cells during their differentiation into myofibroblasts. It was reported that HUVECs undergo EndMT by TGF-β2 stimulation and they can be used as a cell model for myofibroblasts derived from cells that have undergone EndMT (46). We thus examined whether MFG-E8 expression was increased in HUVECs stimulated by TGF-β2. The stimulation induced *Acta2* and *Adam12* expression in the cells, similarly to TGF-β1–treated resident fibroblasts, indicating that they acquired myofibroblast-like properties (Figure 8C and Supplemental Figure 15A). In the TGF-β2–stimulated HUVECs, *Mfge8* expression was induced, and the expression was inhibited by treatment with siRNA against SRF (Figure 8C). These results indicated MFG-E8 was induced in HUVECs by TGF-β via SRF, suggesting that myofibroblasts differentiated from resident fibroblasts and EndMT cells share common TGF-β/SRF–dependent machinery for MFG-E8 production.

To examine whether mechanisms of MFG-E8 production in vitro apply in vivo, we treated myofibroblasts isolated from infarcted mouse hearts with CCG-1423 or siRNA against SRF and evaluated *Mfge8* expression. CCG-1423 (Figure 8D) and siRNA (Figure 8E) treatment significantly attenuated *Mfge8* expression as well as *Acta2* expression. We also confirmed that the expression of TGF-β1 and TGF-β2 was selectively increased in infarcted areas (Supplemental Figure 15B). These results suggested that MFG-E8 production in myofibroblasts is mediated by the TGF-β/SRF pathway.

MFG-E8 administration improves the conditions of hearts after MI. We revealed a protective role of engulfment by cardiac myofibroblasts via MFG-E8 against MI. Because MFG-E8 is a secreted protein, it can be administered to infarcted mouse hearts. Therefore, we examined whether MFG-E8 treatment after MI leads to recovery of infarcted hearts. Ultrapurified recombinant mouse MFG-E8 protein was intramyocardially administered to WT mice immediately after surgery to induce MI (Figure 9A). Evans blue/tetrazolium chloride staining revealed that the areas at risk and the infarct size were comparable between PBS-treated mice and MFG-E8–treated mice during the initial phase after MI (Supplemental Figure 16A). However, 3 days after surgery, we found fewer TUNEL-positive cells in the infarcted areas of MFG-E8–treated mice, suggesting that dead cells were efficiently removed by MFG-E8 treatment (Figure 9B). Furthermore, MFG-E8 administration significantly attenuated the upregulation of inflammatory genes (*Il1b* and *Cxcl2*) that occurred after surgery to induce MI in a concentration-dependent manner (Figure 9C). Consistent with these results, MFG-E8 administration improved survival rates after MI, although the difference was not statistically significant (Supplemental Figure 16B). The favorable effects by MFG-E8 administration were not so prominent in normal hearts (Figure 9, B and C), suggesting a critical role of MFG-E8 in MI. On the oth-

er hand, the expression levels of αSMA (*Acta2*) and integrin $\alpha_v\beta_5$ (*Itgav*, *Itgb5*) were not affected by MFG-E8 treatment (Supplemental Figure 16C), indicating that this did not influence the number of cardiac fibroblasts. We also found that MFG-E8 administration did not induce the mobilization of myofibroblasts in tissues other than the heart, confirming that the effects of MFG-E8 were heart specific (Supplemental Figure 17). These results demonstrated that MFG-E8 treatment promoted the engulfment of dead cells in the infarcted area, resulting in the reduction of secondary necrosis and inflammatory responses in the area.

We next examined whether the effects of MFG-E8 administration on infarcted hearts were mediated by the MFG-E8/integrin engulfment pathway. It was previously reported that the MFG-E8 D89E mutant failed to bind integrins and inhibited the engulfment of apoptotic cells by masking exposed phosphatidylserine (24). We administered recombinant MFG-E8 D89E protein to mice after MI. The survival rate after MI was reduced by MFG-E8 D89E treatment, although the difference was not statistically significant (P = 0.30, Supplemental Figure 18A). The number of TUNEL-positive cells in infarcted areas of the heart in MFG-E8 D89E–treated mice was increased (Supplemental Figure 18B) along with the degree of inflammation in the infarcted area (Supplemental Figure 18C), indicating that the salutary effect of MFG-E8 on the infarcted heart involves MFG-E8–mediated engulfment.

We next assessed whether cardiac morphology and function in infarcted mice were improved by MFG-E8 treatment. MFG-E8 treatment did not affect the morphology and function of normal mouse hearts (Figure 9, C–G, and Supplemental Figure 16D). However, echocardiographic measurements performed on the hearts of PBS-treated and MFG-E8–treated mice at 2, 6, 8, and 10 weeks after MI showed that MFG-E8 treatment significantly attenuated the deterioration of cardiac morphology and function after MI (Figure 9D). Consistently, catheter-based measurements 10 weeks after MI indicated that the intramyocardial administration of MFG-E8 improves cardiac function (Figure 9E). Significant decreases in heart weight and infarct area were also observed in MFG-E8–administered mice 10 weeks after MI (Figure 9, F and G). In contrast, treatment with MFG-E8 D89E reduced cardiac function and increased infarct area and heart weight after MI (Supplemental Figure 18, D–G). These findings indicated that MFG-E8 treatment improved the condition of the heart after MI by promoting the engulfment of dead cells, suggesting that MFG-E8 could be a new therapeutic target for the treatment of MI in the future.

Discussion

To date, dead cells generated in MI were believed to be removed only by infiltrating immune cells, such as macrophages and dendritic cells recruited to the infarcted area (5, 8). Our study identified myofibroblasts as responsible for the removal of dead cells in MI (Figure 10). Cardiac engulfment was found to be dependent on MFG-E8. Myofibroblasts engulf dead cells and acquire antiinflammatory properties upon engulfment, similar to macrophages. Both macrophage-like properties of cardiac myofibroblasts greatly contribute to limiting the size of the infarcted area. In fact, in the infarcted area of MFG-E8 KO mice, the number of unengulfed dead cells was increased and the resultant exaggerated inflammation was induced, which led to a decrease in the number of myofibroblasts at the infarcted area as well as decreases in wall thickness and survival rate after MI (47, 48) (Figure 5, Figure 6, and Supplemental Figure 10). Based on evidence that macrophages that infiltrate the infarcted area contribute to the clearance of dead cells by using Mer, a phagocytic receptor (8), we hypothesized that infiltrated macrophages and myofibroblasts cooperate with each other to remove dead cells by using different molecules in the infarcted heart. In the infarcted area, an abundance of dead cells is rapidly generated. Thus, it is reasonable to assume that myofibroblasts differentiated from resident fibroblasts, which originally reside near dead cardiomyocytes, actively participate in the removal of dead cells. In our study, we used MFG-E8 KO mice for experiments because MFG-E8 is expressed in myofibroblasts, but not cardiomyocytes or inflammatory cells, in infarcted areas of the heart. However, to understand the precise contribution of myofibroblasts to the elimination of dead cells in MI via MFG-E8–mediated engulfment, myofibroblast-specific MFG-E8 conditional KO mice would be useful. Similarly to what occurs in MI, we assume that myofibroblasts that appear in other damaged tissues also actively contribute to elimination of dead cells and attenuation of inflammation. In fact, we found that MFG-E8 is also expressed in myofibroblasts in a mouse model of liver injury (Supplemental Figure 19). It will be interesting to examine whether myofibroblasts in other tissues have the ability to engulf apoptotic cells and express engulfment-related molecules, including MFG-E8.

Myofibroblasts have long been known to facilitate fibrosis. In the current model of tissue repair after injury, myofibroblasts are believed to produce extracellular matrix proteins only after they receive cytokines released from macrophages that recognize dead cells and "danger signals," such as inflammatory mediators leaked from dead cells at injury sites (49). However, the finding that cardiac myofibroblasts appear after MI, engulf dead cells, and acquire macrophage-like antiinflammatory properties upon engulfment raises the possibility that engulfment by myofibroblasts itself triggers the production of extracellular matrix proteins without the assistance of macrophages. In this regard, it will be of great value to examine whether engulfment by cardiac myofibroblasts influences the production of extracellular matrix proteins to reassign the role of myofibroblasts in tissue repair and subsequent fibrosis development. It was recently reported that the autophagy machinery in macrophages is recruited to phagosomes containing dead cells and regulates the expression of proinflammatory genes, a process that requires the autophagy-related molecule ATG-7 (50). If this also occurs in cardiac myofibroblasts, it could modulate the production of extracellular matrix proteins. Interestingly, *Atg7* expression was increased in infarcted hearts, an effect that was attenuated in MFG-E8 KO mice, raising the possibility that MFG-E8 influences autophagy (Supplemental Figure 20).

Myofibroblasts have been considered to have diverse functions because they originate from multiple cell types (11–13). However, only a few proteins have been reported to be involved in determining functional differences between cardiac myofibroblasts. The results of the present study indicate that MFG-E8 was produced only by a population of myofibroblasts differentiated from resident fibroblasts and cells that had undergone EndMT

among the 5 cellular origins of cardiac myofibroblasts. Therefore, MFG-E8 can be potentially used as a new marker that characterizes cardiac myofibroblasts that appear after MI. MFG-E8 expression may endow a special engulfment activity to a subset of cardiac myofibroblasts. Future studies examining the engulfment ability of non–MFG-E8–producing cardiac myofibroblasts will clarify this point and elucidate functional differences in a variety of myofibroblasts that appear in MI.

So far, none of the proteins involved in the removal of dead cells following MI have been reported as potential therapeutic targets for the treatment. Here, we demonstrated that MFG-E8 administration substantially improved cardiac function after MI. However, further optimization in MFG-E8 administration methods remains to be examined in detail to maximize its effects on infarcted hearts. MFG-E8 treatment can also be used in combination with other emerging candidates for treatments that target molecules other than those involved in engulfment (51).

Methods

Mice. Eight- to ten-week-old male WT (C57BL/6) (Charles River) and MFG-E8 KO mice (backcrossed for more than 7 generations on the C57BL/6 background) (24) were used in the study.

MI. Mice were anesthetized with pentobarbital (50 mg/kg) and subjected to permanent occlusion of the left coronary artery.

Culture and isolation of cardiac cells. At 3 days after operation, the ventricles of MI-operated mice were digested with PBS containing 0.1% collagenase A (Roche Diagnostics) and 0.1% trypsin (Sigma-Aldrich) at 37°C with agitation. Cells were placed in plates containing 10% FBS/DMEM overnight, and the culture medium was then changed to remove the unattached cells. The attached cells were cultured for more than 6 days and used as myofibroblasts in our in vitro experiments. We used myofibroblasts from passage 1 (P1) throughout our study. Myofibroblasts were transfected with siRNA using Lipofectamine 2000 (Invitrogen). All validated siRNAs were purchased from Ambion. The target sequence for human *SRF* was 5′-UGAUGUACCCUAGCCCGCATT-3′, while that for mouse *Srf* was 5′-GCCUUUUCACGGUUUCUUUTT-3′. Silencer Select Negative Control no. 1 siRNA was used as control in each experiment (Thermo Fisher Scientific).

Neonatal cardiac fibroblasts and cardiomyocytes were isolated from the heart ventricles of 2-day-old Sprague-Dawley rats (Kyudo Laboratories). The ventricles were digested with Liberase Research Grade (Roche Diagnostics). The digested cells were plated on dishes and incubated for 1 hour at 37°C, and adherent and nonadherent cells were harvested as cardiac fibroblasts and cardiomyocytes, respectively.

HUVECs purchased from ATCC were grown in endothelial cell growth medium-2 (Lonza) on collagen I–coated plates (BD Biosciences). The cells were transfected with siRNA targeting human SRF or control scrambled siRNA using Lipofectamine 2000. At 24 hours after transfection, the HUVECs were starved with human endothelial serum-free medium-2 (Invitrogen) for 24 hours. These cells were then cultured in human endothelial SFM with or without TGF-β2 (R&D Systems) for 3 days.

Production of AAV9-cTnT-EGFP. HEK293 cells were cotransfected with an AAV transgene plasmid (pENN-PI-cTnT-eGFP-WPRE-rBG) and 2 helper plasmids (pXR9 and pXX6-80) using polyethylenimine "Max" (Polysciences). The AAV transgene plasmid pENN-cTnT-PI-eGFP-WPRE-rBG was purchased from Penn Vector Core. The AAV serotype helper plasmid pXR9 and the adenoviral helper plasmid pXX6-80 were gifts from J. E. Rabinowitz (Temple University, Philadelphia, Pennsylvania, USA). AAV was purified with ultracentrifugation as previously reported, with some modifications (29). The virus titer was determined by real-time RT-PCR (52).

In vivo phagocytosis assay. Virus carrying the cDNA for EGFP was diluted in PBS to adjust the viral titer (cTnT-EGFP-AAV9 = 1×10^{12} copies/μl), and 20 μl of the viral solution was injected in 3-day-old mice (by subcutaneous injection) with 29-gauge needles (BD Biosciences). Eight to ten weeks after injection, mice were subjected to the MI operation. For FACS analysis, at 3 days after operation, hearts were digested using a cocktail of collagenase type II (CLS2) (Worthington) and elastase (ESL) (Worthington) in PBS at 37°C with agitation. After digestion, cells were stained with eFluor780 dye (1:1000, 65-0865; eBioscience) and phycoerythrin-conjugated (PE-conjugated) anti-CD11b (1:200, M1/70; BioLegend), and allophycocyanin-conjugated (APC-conjugated) anti–PDGFRα (1:200, 5A5; BioLegend) antibodies were added. Stained cells were sorted with a FACSAria III (BD Biosciences).

For immunohistochemical analyses, the hearts of WT, MFG-E8 KO, and AAV9-cTnT-EGFP–administered mice 3 days after MI were fixed in 4% PFA, embedded in OCT compound (Sakura FineTek), and cut into 6-μm–thick sections using a cryostat (Leica Microsystems). The sections were labeled with Cy3-conjugated anti-αSMA (1:400, 1A4; Sigma-Aldrich), anti-GFP (1:300, ab13970; Abcam), and anti-cardiac troponin I3 (TNNI3) (1:200, ab56357; Abcam) antibodies. Images were captured using a confocal microscope (LSM700, Zeiss). Over 1200 αSMA-positive cells were evaluated, and engulfment capacity was determined by dividing the number of engulfed apoptotic cells by the area of αSMA-positive cells, averaged from 5 to 11 randomly selected fields.

Labeling of necroptotic cardiomyocytes with AAV. AAV9-expressing RIP3-EGFP under the control of the *cTnT* promoter was administered intramyocardially to 7-week-old WT mice (4×10^{12} copies/mouse). Mice expressing RIP3-EGFP specifically in cardiomyocytes (10 weeks old) were subjected to MI. Three days after the operation, their hearts were fixed in 4% PFA. Cryostat sections were labeled with Cy3-conjugated anti-αSMA (1:400) and anti-GFP (1:300) antibodies.

Electron microscope. The infarct and border areas of infarcted hearts 3 days after MI were dissected and immersed in 2% PFA and 2% glutaraldehyde buffered with 0.1 M phosphate buffer at 4°C overnight. Samples were post-fixed with 2% OsO_4 in 0.1 M phosphate buffer at 4°C for 2 hours. Tissue samples were then dehydrated in a graded series of ethanol and embedded in Quetol-812 (Nisshin EM). Ultrathin sections were prepared on an ultramicrotome (EM UC7; Leica) and stained with 2% uranyl acetate and lead citrate. Sections were visualized by transmission electron microscopy (Tecnai 20, FEI Co.).

RT-PCR. Total RNA of various tissues was extracted from WT or MFG-E8 KO mice using Isogen (Nippon Gene) and purified using an RNeasy Plus Mini Kit (QIAGEN). Total RNA was isolated from neonatal rat cardiac fibroblasts, mouse myofibroblasts, and HUVECs using an RNeasy Micro Kit (QIAGEN). RT-PCR was carried out using a One Step PrimeScript RT-PCR Kit (Takara Bio) on a 7500 Fast Real-Time PCR System (Applied Biosystems). The following TaqMan probes were purchased from Applied Biosystems: *Mfge8* (Mm00500549_m1), *Mfge8* (Rn00563082_m1), *Mfge8* (Hs00170712_m1), *Itgav* (Mm00434486_m1), *Itgb5*

(Mm00439825_m1), *Tnfα* (Mm00443258_m1), *Il1b* (Mm00434228_m1), *Acta2* (Rn01759928_g1), *Acta2* (Mm00725412_s1), *Acta2* (Hs00426835_g1), *Adam12* (Rn01479221_m1), *Adam12* (Mm00475719_m1), *Srf* (Mm00491032_m1), *Tgfb1* (Mm01178820_m1), *Tgfb2* (Mm00436955_m1), *Ctgf* (Mm01192932_g1), and eukaryotic 18S rRNA (Hs03003631_g1). Other primer sequences used for real-time RT-PCR included the following: *Il6* (forward: 5′-GGGACTGATGCTGGTGACAA-3′, reverse: 5′-TGCCATTGCACAACTCTTTTCT-3′, probe: 5′-TCACAGAGGATACCACTCCCAACAGACCTG-3′); macrophage inflammatory protein-2 (*Cxcl2*) (forward: 5′-CGCTGTCAATGCCTGAAGAC-3′, reverse: 5′-CCTTGAGAGTGGCTATGACTTCTG-3′, probe: 5′-TCCAGAGCTTGAGTGTGACGCCCC-3′); *Gas6* (forward: 5′-CCTGCCAGAAGTATCGGTGATT-3′, reverse: 5′-CCCGTTTACCTCCAGAGTCATG-3′, probe: 5′-CACCCGTCACTGCGTTCTACCGC-3′), *Mertk* (forward: 5′-CTGCATGTTGCGGGATGAC-3′, reverse: 5′-ACTTCACAGGCATTTTGGCAAT-3′, probe: 5′-CTGCGTGGCAGACTTTGGCCTCTC-3′); *Timd4* (forward: 5′-CCCAGAGCTGCTTCCAACA-3′, reverse: 5′-CAGGCAGAGTTTCTGATTCTGTAGTG-3′, probe: 5′-ACACTAGCCACCACTGCCTTCAGTACAGCA-3′); *Stab2* (forward: 5′-CACTGACCGGAGTTCTCATTCC-3′, reverse: 5′-ACCAATTTTCAGGTTCCATGCT-3′, probe: 5′-TCGGAGCCCACGGCAATCTTCAC-3′); matrix metalloproteinase-9 (*Mmp9*) (forward: 5′-GGCCCCAGGAGTCTGGATA-3′, reverse: 5′-AATAGGCTTTGTCTTGGTACTGGAA-3′, probe: 5′-ACCCACGTCAGCGGGCTTCTCC-3′); *Wt1* (forward: 5′-GAGCAACCACGGCACAGG-3′, reverse: 5′-GCTGACCGGACAAGAGTTGG-3′, probe: 5′-CTCCAGATACACGCCGCACATCCTGAATG-3′); *Tbx18* (forward: 5′-CTACGGACTCTCACCTTTGAAGATA-3′, reverse: 5′-TGAGGATGTGTAGCAGGGACA-3′, probe: 5′-CCCAAAGCAAGGCAACACAAGTTCTTCAGC-3′); *Snai1* (forward: 5′-CCGCCGGAAGCCCAACTA-3′, reverse: 5′-TGAGGGTGGGCAGCGAAG-3′, probe: 5′-CGTGTGTGGAGTTCACCTTCCAGCAGC-3′); *Atg7* (forward: 5′-CTCACCAGATCCGGGGTTTTC-3′, reverse: 5′-GAATCCTTCTCGCTCGTACTGA-3′, probe: 5′-TTCGATAATGTTCTTCCTGTCAGCCTGGCA-3′); *Becn1* (forward: 5′-CAAGCTCAAGAAAACCAATGTCTTC-3′, reverse: (5′-CAGGCAGCATTGATTTCATTCCA-3′, probe: 5′-CCTTCCACATCTGGCACAGCGGACAGT-3′); and *Gapdh* (forward: 5′-TGCCCCCATGTTTGTGATG-3′, reverse: 5′-GGCATGGACTGTGGTCATGA-3′, probe: 5′-ACCACCAACTGCTTAGCCCCCCTG-3′)

The results were normalized to GAPDH or 18S rRNA.

Flow cytometry. Isolated cardiac myofibroblasts were harvested with accutase treatment and subsequently stained with the following antibodies: PE–anti-CD45 (1:200, 30-F11, BioLegend), APC–anti-CD68 (1:200, FA-11, BioLegend), FITC–anti-αSMA(1:200, 1A4; Sigma-Aldrich), peridinin chlorophyll protein (PerCP)/eFluor710–anti–MHC class II (1:200, 46-5321-80; eBioscience), anti-SM22α antibody (1:200, ab14106; Abcam), APC–anti-PDGFRα (1:200, APA5; BioLegend), and PE–anti-integrin α_v (1:200, RMV-7; BioLegend) antibody. For αSMA and SM22α staining, cells were permeabilized with 0.5% saponin before staining. For MFG-E8 labeling, cells were incubated with PerCP/Cy5.5–anti-CD31 (1:100, 390; BioLegend) and PE–anti-CD21/CD35 (1:100, 7E9; BioLegend) antibodies, followed by permeabilization with 0.5% saponin. Cells were then labeled with anti–MFG-E8 (1:200, 2422; MBL), anti-vimentin (1:100, GP53; Progen), and FITC-conjugated anti-αSMA (1:200, 1A4; Sigma-Aldrich) antibodies. Alexa Fluor 647–conjugated anti-hamster IgG, Alexa Fluor 488–conjugated anti-guinea pig IgG (both from Jackson ImmunoResearch), or Alexa Fluor 488–conjugated anti-rabbit IgG (Invitrogen) was used as a secondary antibody for anti–MFG-E8, anti-vimentin, and anti-SM22α antibodies, respectively. The stained cells were analyzed using FACSCalibur or FACSAria III.

Western blot analysis. Hearts of mice were homogenized in a lysis buffer (50 mM Tris-Cl [pH 8.0], 150 mM NaCl, 1.0% NP-40, 0.5% sodium deoxycholate, 1 mM Na_3VO_4, 1 mM NaF) containing protease inhibitors (Nacalai). Lysed tissues were subjected to Western blotting using anti–MFG-E8 (1:2,000, 18A2-G10; MBL) followed by HRP–anti-hamster IgG secondary antibody (1:5,000, Santa Cruz Biotechnology Inc.), and bands were visualized using the ECL System (PerkinElmer).

Immunohistochemistry and immunocytochemistry. Hearts of WT or MFG-E8 KO mice, livers of CCl_4-injected mice, and spleens of WT mice were excised. The cryostat sections were fixed in acetone and incubated overnight at 4°C with the following primary antibodies: anti–MFG-E8 (1:200, 18A2-G10; MBL), anti-vimentin (1:100, GP53; Progen), Cy3-conjugated anti-αSMA (1:400, 1A4; Sigma-Aldrich), anti-CD31 (1:100, 550513; BD Biosciences), FITC-conjugated anti–Gr-1 (1:200, RB6-8C5; BioLegend), anti-CD68 (1:200, MCA1957; AbD Serotec), anti–PDGFR-β (1:100, APB5; eBioscience), anti–Wt-1 (1:200, sc-192; Santa Cruz Biotechnology Inc.), biotin-conjugated anti-CD21/CD35 (1:200, 7E9; BioLegend), and anti-S100A4 (1:100, Ab-8; Neomarkers). Integrin β_5 (1:200, ab15459; Abcam) staining was performed on 6-μm–thick sections of MI-operated hearts fixed in 4% PFA at 4°C. Images were captured and analyzed using an epifluorescence microscope (BZ-9000; Keyence) and a confocal microscope (A1Rsi; Nikon).

Paraffin-embedded heart sections of patients who had undergone MI were deparaffinized and autoclaved in 10 mM citrate buffer (pH 6.0) at 121°C for 10 minutes for antigen retrieval. The sections were treated with 0.3% H_2O_2/MeOH solution for 10 minutes and subsequently blocked with PBS containing 10% normal goat serum. Next, the sections were stained by mouse monoclonal anti-human MFG-E8 antibody (1:200) (53) and rabbit anti-αSMA antibody (1:200, EPR5368; Epitomics) and visualized using a biotin-streptavidin-peroxidase kit (LSAB 2 kit; DAKO). Quantitative analysis was performed using ImageJ (NIH) software. All stained sections were observed under a light microscope (BX50; Olympus), fluorescence microscope, or confocal microscope (FV10i; Olympus).

Myofibroblasts cultured in an 8-well slide chamber were fixed in acetone and incubated overnight at 4°C with anti-SM22α (1:200, ab14106; Abcam) and anti–MFG-E8 (1:200, 18A2-G10; MBL) antibodies.

TUNEL staining with an αSMA- or CD68-specific antibody. Hearts, lungs, livers, spleens, and kidneys were excised from MI-operated mice and fixed in 4% PFA at 4°C. Sections were stained with Cy3-conjugated anti-αSMA (1:400, 1A4; Sigma-Aldrich) or anti-CD68 (1:200, MCA1957GA; AbD Serotec) antibody at 4°C. TUNEL staining (Millipore) was performed according to the manufacturer's instructions. Over 70 engulfed apoptotic cells were evaluated, and engulfment capacity was determined by dividing the number of these cells by the area of αSMA-positive (or CD68) cells, averaged from 8 to 10 randomly selected fields.

Bone marrow transfer experiment. We lethally irradiated (10 Gy) recipient male MFG-E8 KO mice. Bone marrow cells were isolated from male WT mice by flushing the tibias and femurs. Recipient MFG-E8 KO mice were administered donor bone marrow cells through the orbital vein. Reconstitution efficiency was assessed by staining of blood leukocytes prepared from the transplanted mice with

FITC–anti-CD45.1 (1:200, A20; BioLegend) and APC–anti-CD45.2 (1:200, 104; BioLegend) after 5 weeks. Percentage of chimerism in the blood was determined for all monocytes.

Phagocytosis assay of apoptotic cells in cardiac macrophages and cardiac myofibroblasts. At 3 days after operations, hearts were excised from MI-operated WT mice and digested using a cocktail of 4.4 mg/ml Dispase II (Sigma-Aldrich), 2.5 mg/ml trypsin, and 1 mM EDTA in PBS at 37°C with agitation. After digestion, cells were stained with eFluor 780 viability dye for 30 minutes. The following antibodies were then added, and the reaction was allowed for 30 minutes: FITC anti-Ly-6C (1:100, HK1.4; BioLegend), PE anti-Ly-6G (1:200, 1A8; BioLegend), PerCP/Cy5.5 anti-CD11b (1:200, M1/70; BioLegend), and APC anti-F4/80 (1:100, BM8; BioLegend). The stained cells were analyzed, and cardiac macrophages ($Ly\text{-}6G^-/CD11b^+/Ly\text{-}6C^{lo}/F4/80^{hi}$) were sorted by FACSAria III. Sorted macrophages (5×10^4 cells/well) and adult mouse cardiac myofibroblasts (1×10^4 cells/well) were cultured in an 8-well slide chamber coated with poly-L-lysine (Sigma-Aldrich). For the phagocytosis assay, thymocytes were collected from female C57BL/6 mice, labeled with 5-chloromethylfluorescein diacetate (CMFDA), pHrodo Red succinimidyl ester (P36600; Thermo Fisher Scientific), or CellTrace Far Red dye (C34564; Thermo Fisher Scientific), and treated with 10 μM dexamethasone at 37°C for 4.5 hours to induce apoptosis (26). CMFDA-labeled apoptotic thymocytes were cocultured with cardiac macrophages or cardiac myofibroblasts at 37°C, after which the slides were washed vigorously with PBS to remove the attached apoptotic thymocytes. The slides were fixed in 1% PFA and mounted in FluorSave mounting medium (Calbiochem). Phagocytosis was evaluated under a phase-contrast microscope as reported previously (20). Over 150 myofibroblasts were evaluated, and the phagocytosis index was determined as the number of apoptotic cells engulfed per macrophage (or myofibroblast).

Phagocytosis assay of necroptotic cells in cardiac myofibroblasts. To prepare necroptotic cells, L929 cells (Riken BioResource Center) were labeled with CMFDA under serum-free conditions and then treated with 20 μM Z-Val-Ala-Asp(OMe)-CH_2F (Z-VAD-FMK) (a gift from M. Sodeoka and K. Dodo [Riken]) at 37°C for 2 hours in DMEM supplemented with 10% FBS prior to addition of human TNF-α (10 ng/ml) (Peprotech). Floating L929 cells were harvested as necroptotic cells 4.5 hours after TNF-α stimulation. CMFDA-labeled necroptotic L929 cells (2×10^5 cells/well) were cocultured with cardiac myofibroblasts (2×10^4 cells/well) in an 8-well chamber slide for 3 hours at 37°C. Phagocytosis was evaluated by phase-contrast microscopy.

Recombinant MFG-E8 preparation and administration. Recombinant MFG-E8 (WT) and MFG-E8 (D89E) were prepared as previously reported (16). Mice were intramyocardially administered 20 μl (2 doses of 10 μl each) MFG-E8 or MFG-E8 D89E solution or PBS immediately after ligation of the left anterior descending coronary artery, using 29-gauge needles (BD Biosciences).

Echocardiographic analysis and hemodynamic measurement. Transthoracic ultrasound cardiography and hemodynamic measurements were performed on mice under anesthesia after sham or MI operation as previously reported (54).

Histological analysis. Infarct hearts were fixed in 10% neutral-buffered formalin and embedded in paraffin. Ventricular sections were stained with Masson's trichrome, H&E, and PicroSirius red and observed under a microscope. The infarct/left ventricular (LV) area, collagen volume fraction at the infarct area, and myocardial wall thickness of the infarct area were analyzed using a BZ-II analyzer (Keyence). Wall thickness was determined at 3 points of the LV for each group.

Assessment of infarct size. The initial infarct size was assessed 3 hours after MI using Evans blue dye and TTC staining as previously reported (54). The necrotic area (TTC negative) was represented as a percentage of AAR (area not stained with Evans blue dye), while the AAR was represented as a percentage of the LV area.

Statistics. We used GraphPad Prism 6.0 software for all statistical analyses. Data represent the mean ± SEM of at least 3 independent experiments. Two-tailed Student's *t* tests were used for 2-group comparisons, and ANOVA with the Student–Newman-Keuls test was used for multiple-group comparisons. Differences were considered significant at $P < 0.05$. No statistical method was used to predetermine sample size. Intergroup differences in survival rate were tested by the log-rank test. The experiments were randomized, and the researchers were not blinded to allocation during experiments and outcome analysis, except for histological experiments, echocardiographic analysis, and hemodynamic measurements.

Study approval. All animal experiments were performed using approved protocols and in accordance with the guidelines of Kyushu University. Mice were housed in accordance with the Institutional Animal Care and Use Committee regulations at Kyushu University. This study using human autopsy specimens was performed under the informed consent of the participants, following the ethical guideline of Tokyo Medical University.

Author contributions

M Nakaya conceived the project, designed the project, performed experiments, and analyzed and interpreted data. KW, MT, SM, H Ohara, HN, M Nishida, YH, and H Ono performed some in vivo and in vitro experiments and helped with data interpretation. KW, MT, TN, H Ohara, HN, YH, H Ono, and AT performed animal surgery. AH purified MFG-E8 protein. TN and MK analyzed human samples. HY, AN, AT, GI, MT, RI, KI, and SN provided key reagents and contributed to the scientific discussion. M Nakaya and HK wrote the paper.

Acknowledgments

We thank K. Fujita (Tokyo Medical University) for his expert assistance. This study was supported by grants from the Ministry of Education, Culture, Sports, Science, and Technology of Japan (MEXT) (25713007 to M Nakaya and 25253011 to HK); Grant-in-Aid for Scientific Research on Innovative Areas (Homeostatic regulation by various types of cell death, and High definition physiology project) MEXT (15H01383 to M Nakaya and 22136008 to M Nakaya, GI, and RI); Kyushu University Interdisciplinary Programs in Education and Projects in Research Development (P&P) (to M Nakaya); the Japan Heart Foundation/Novartis Grant for Research Award on Molecular and Cellular Cardiology 2014, the Takeda Science Foundation, the Naito Foundation, the Mochida Memorial Foundation for Medical and Pharmaceutical Research, the Suzuken Memorial Foundation, the Astellas Foundation for Research on Metabolic Disorders, the Kanae Foundation for the Promotion of Medical Science, the Kaibara Morikazu Medical Science Promotion Foundation, MSD Life Science Foundation, and the Nakajima Foundation

(to M Nakaya); the Platform Project for Supporting Drug Discovery and Life Science Research (Platform for Drug Discovery, Informatics, and Structural Life Science) the MEXT and the Japan Agency for Medical Research and development (AMED); and the Funding Program for Next Generation World-Leading Researchers (NEXT Program) (to MT). We appreciate the technical support from the Research Support Center, Graduate School of Medical Sciences, Kyushu University and from the Medical Institute of Bioregulation, Kyushu University.

Address correspondence to: Michio Nakaya, Department of Pharmacology and Toxicology, Graduate School of Pharmaceutical Sciences, Kyushu University, 3-1-1 Maidashi, Higashi-ku, Fukuoka 812-8582, Japan. Phone: 81.92.642.6878; E-mail: nakaya@phar.kyushu-u.ac.jp.

1. Roger VL, et al. Heart disease and stroke statistics--2012 update: a report from the American Heart Association. *Circulation*. 2012;125(1):e2–e220.
2. Yellon DM, Hausenloy DJ. Myocardial reperfusion injury. *N Engl J Med*. 2007;357(11):1121–1135.
3. Olivetti G, et al. Apoptosis in the failing human heart. *N Engl J Med*. 1997;336(16):1131–1141.
4. Whelan RS, Kaplinskiy V, Kitsis RN. Cell death in the pathogenesis of heart disease: mechanisms and significance. *Annu Rev Physiol*. 2010;72:19–44.
5. Frangogiannis NG. Regulation of the inflammatory response in cardiac repair. *Circ Res*. 2012;110(1):159–173.
6. Muñoz LE, Lauber K, Schiller M, Manfredi AA, Herrmann M. The role of defective clearance of apoptotic cells in systemic autoimmunity. *Nat Rev Rheumatol*. 2010;6(5):280–289.
7. Nagata S, Hanayama R, Kawane K. Autoimmunity and the clearance of dead cells. *Cell*. 2010;140(5):619–630.
8. Wan E, et al. Enhanced efferocytosis of apoptotic cardiomyocytes through myeloid-epithelial-reproductive tyrosine kinase links acute inflammation resolution to cardiac repair after infarction. *Circ Res*. 2013;113(8):1004–1012.
9. Frangogiannis NG. The immune system and cardiac repair. *Pharmacol Res*. 2008;58(2):88–111.
10. Wynn TA. Integrating mechanisms of pulmonary fibrosis. *J Exp Med*. 2011;208(7):1339–1350.
11. Gabbiani G. The myofibroblast in wound healing and fibrocontractive diseases. *J Pathol*. 2003;200(4):500–503.
12. Porter KE, Turner NA. Cardiac fibroblasts: at the heart of myocardial remodeling. *Pharmacol Ther*. 2009;123(2):255–278.
13. Zeisberg M, Kalluri R. Cellular mechanisms of tissue fibrosis. 1. Common and organ-specific mechanisms associated with tissue fibrosis. *Am J Physiol, Cell Physiol*. 2013;304(3):C216–C225.
14. Krenning G, Zeisberg EM, Kalluri R. The origin of fibroblasts and mechanism of cardiac fibrosis. *J Cell Physiol*. 2010;225(3):631–637.
15. Akakura S, et al. The opsonin MFG-E8 is a ligand for the alphavbeta5 integrin and triggers DOCK180-dependent Rac1 activation for the phagocytosis of apoptotic cells. *Exp Cell Res*. 2004;292(2):403–416.
16. Hanayama R, Tanaka M, Miwa K, Shinohara A, Iwamatsu A, Nagata S. Identification of a factor that links apoptotic cells to phagocytes. *Nature*. 2002;417(6885):182–187.
17. Heidt T, et al. Differential contribution of monocytes to heart macrophages in steady-state and after myocardial infarction. *Circ Res*. 2014;115(2):284–295.
18. Hirschi KK, Rohovsky SA, D'Amore PA. PDGF, TGF-beta, and heterotypic cell-cell interactions mediate endothelial cell-induced recruitment of 10T1/2 cells and their differentiation to a smooth muscle fate. *J Cell Biol*. 1998;141(3):805–814.
19. Tomasek JJ, Gabbiani G, Hinz B, Chaponnier C, Brown RA. Myofibroblasts and mechano-regulation of connective tissue remodelling. *Nat Rev Mol Cell Biol*. 2002;3(5):349–363.
20. Nakaya M, Kitano M, Matsuda M, Nagata S. Spatiotemporal activation of Rac1 for engulfment of apoptotic cells. *Proc Natl Acad Sci U S A*. 2008;105(27):9198–9203.
21. Kung G, Konstantinidis K, Kitsis RN. Programmed necrosis, not apoptosis, in the heart. *Circ Res*. 2011;108(8):1017–1036.
22. Wu YT, Tan HL, Huang Q, Sun XJ, Zhu X, Shen HM. zVAD-induced necroptosis in L929 cells depends on autocrine production of TNFα mediated by the PKC-MAPKs-AP-1 pathway. *Cell Death Differ*. 2011;18(1):26–37.
23. Voll RE, Herrmann M, Roth EA, Stach C, Kalden JR, Girkontaite I. Immunosuppressive effects of apoptotic cells. *Nature*. 1997;390(6658):350–351.
24. Hanayama R, et al. Autoimmune disease and impaired uptake of apoptotic cells in MFG-E8-deficient mice. *Science*. 2004;304(5674):1147–1150.
25. Kranich J, et al. Follicular dendritic cells control engulfment of apoptotic bodies by secreting Mfge8. *J Exp Med*. 2008;205(6):1293–1302.
26. Nakaya M, et al. GRK6 deficiency in mice causes autoimmune disease due to impaired apoptotic cell clearance. *Nat Commun*. 2013;4:1532.
27. Gabbiani G, Ryan GB, Majne G. Presence of modified fibroblasts in granulation tissue and their possible role in wound contraction. *Experientia*. 1971;27(5):549–550.
28. Prasad KM, Xu Y, Yang Z, Acton ST, French BA. Robust cardiomyocyte-specific gene expression following systemic injection of AAV: in vivo gene delivery follows a Poisson distribution. *Gene Ther*. 2011;18(1):43–52.
29. Zincarelli C, Soltys S, Rengo G, Rabinowitz JE. Analysis of AAV serotypes 1-9 mediated gene expression and tropism in mice after systemic injection. *Mol Ther*. 2008;16(6):1073–1080.
30. Mizushima N, Ohsumi Y, Yoshimori T. Autophagosome formation in mammalian cells. *Cell Struct Funct*. 2002;27(6):421–429.
31. Declercq W, Vanden Berghe T, Vandenabeele P. RIP kinases at the crossroads of cell death and survival. *Cell*. 2009;138(2):229–232.
32. Luedde M, et al. RIP3, a kinase promoting necroptotic cell death, mediates adverse remodelling after myocardial infarction. *Cardiovasc Res*. 2014;103(2):206–216.
33. Heesters BA, Myers RC, Carroll MC. Follicular dendritic cells: dynamic antigen libraries. *Nat Rev Immunol*. 2014;14(7):495–504.
34. Zeisberg EM, Kalluri R. Origins of cardiac fibroblasts. *Circ Res*. 2010;107(11):1304–1312.
35. Lin SL, Kisseleva T, Brenner DA, Duffield JS. Pericytes and perivascular fibroblasts are the primary source of collagen-producing cells in obstructive fibrosis of the kidney. *Am J Pathol*. 2008;173(6):1617–1627.
36. Balli D, et al. Foxm1 transcription factor is required for lung fibrosis and epithelial-to-mesenchymal transition. *EMBO J*. 2013;32(2):231–244.
37. Zhou B, et al. Adult mouse epicardium modulates myocardial injury by secreting paracrine factors. *J Clin Invest*. 2011;121(5):1894–1904.
38. von Gise A, Pu WT. Endocardial and epicardial epithelial to mesenchymal transitions in heart development and disease. *Circ Res*. 2012;110(12):1628–1645.
39. Zeisberg EM, et al. Endothelial-to-mesenchymal transition contributes to cardiac fibrosis. *Nat Med*. 2007;13(8):952–961.
40. Li J, Qu X, Bertram JF. Endothelial-myofibroblast transition contributes to the early development of diabetic renal interstitial fibrosis in streptozotocin-induced diabetic mice. *Am J Pathol*. 2009;175(4):1380–1388.
41. Davis J, Burr AR, Davis GF, Birnbaumer L, Molkentin JD. A TRPC6-dependent pathway for myofibroblast transdifferentiation and wound healing in vivo. *Dev Cell*. 2012;23(4):705–715.
42. Leask A. Potential therapeutic targets for cardiac fibrosis: TGFbeta, angiotensin, endothelin, CCN2, and PDGF, partners in fibroblast activation. *Circ Res*. 2010;106(11):1675–1680.
43. Dulauroy S, Di Carlo SE, Langa F, Eberl G, Peduto L. Lineage tracing and genetic ablation of ADAM12(+) perivascular cells identify a major source of profibrotic cells during acute tissue injury. *Nat Med*. 2012;18(8):1262–1270.
44. Hinz B, et al. Recent developments in myofibroblast biology: paradigms for connective tissue remodeling. *Am J Pathol*. 2012;180(4):1340–1355.
45. Evelyn CR, et al. CCG-1423: a small-molecule inhibitor of RhoA transcriptional signaling. *Mol Cancer Ther*. 2007;6(8):2249–2260.
46. Medici D, Shore EM, Lounev VY, Kaplan FS, Kalluri R, Olsen BR. Conversion of vascular endothelial cells into multipotent stem-like cells. *Nat Med*. 2010;16(12):1400–1406.
47. Huebener P, et al. CD44 is critically involved in infarct healing by regulating the inflammatory and fibrotic response. *J Immunol*. 2008;180(4):2625–2633.
48. Kempf T, et al. GDF-15 is an inhibitor of leukocyte integrin activation required for survival after myocardial infarction in mice. *Nat Med*. 2011;17(5):581–588.

49. Wynn TA, Ramalingam TR. Mechanisms of fibrosis: therapeutic translation for fibrotic disease. *Nat Med*. 2012;18(7):1028–1040.
50. Martinez J, et al. Microtubule-associated protein 1 light chain 3 alpha (LC3)-associated phagocytosis is required for the efficient clearance of dead cells. *Proc Natl Acad Sci U S A*. 2011;108(42):17396–17401.
51. Qian L, et al. In vivo reprogramming of murine cardiac fibroblasts into induced cardiomyocytes. *Nature*. 2012;485(7400):593–598.
52. Aurnhammer C, et al. Universal real-time PCR for the detection and quantification of adeno-associated virus serotype 2-derived inverted terminal repeat sequences. *Hum Gene Ther Methods*. 2012;23(1):18–28.
53. Yamaguchi H, et al. Milk fat globule EGF factor 8 in the serum of human patients of systemic lupus erythematosus. *J Leukoc Biol*. 2008;83(5):1300–1307.
54. Watari K, Nakaya M, Nishida M, Kim KM, Kurose H. β-arrestin2 in infiltrated macrophages inhibits excessive inflammation after myocardial infarction. *PLoS ONE*. 2013;8(7):e68351.